Thesis for the degree of Licentiate of Engineering

CO_2 activation for methanol synthesis on copper and indium oxide surfaces

Alvaro Posada Borbón

CHALMERS

Department of Physics
Chalmers University of Technology
Gothenburg, Sweden 2019

CO_2 activation for methanol synthesis
on copper and indium oxide surfaces

Alvaro Posada Borbón

Department of Physics
Chalmers University of Technology
SE-412 96 Gothenburg
Sweden
Telephone: +46 (0)31-772 1000

Cover:
Schematic representation of CO_2 activation and reaction on copper and indium oxide surfaces for methanol synthesis.

Printed at Chalmers Reproservice
Gothenburg, Sweden 2019

CO_2 activation for methanol synthesis
on copper and indium oxide surfaces

Alvaro Posada Borbón
Department of Physics
Chalmers University of Technology

Abstract

Catalytic recycling of CO_2 to added-value chemicals, such as methanol (CH_3OH), has been proposed as a possible way for sustainable production of fuel and chemicals, in addition to providing a route to mitigate climate change. Multiple systems are known to be active for the conversion of CO_2 to methanol, and the state of the art catalyst is $Cu/ZnO/Al_2O_3$. This catalyst is, however, known to deactivate rapidly. Moreover, there is no scientific consensus on either the active phase or the reaction mechanism. In response to this, the search for of longer-lasting catalysts for methanol-synthesis has been intense. In recent years, an In_2O_3/ZrO_2 catalyst has attracted much attention, thanks to its high selectivity, activity and durability.

In this thesis, we investigate the surface active phase and its effect on CO_2 adsorption on Cu(100) and In_2O_3(110) with the use of density functional theory (DFT) calculations and *ab-initio* thermodynamics. Our results are compared to ambient pressure X-ray photoelectron emission spectroscopy (XPS) experiments. CO_2 adsorption is the initial step in the reduction process. Hence, understanding of the active catalyst phase, and its effect on the adsorption process, is the first step for the rationalization of the catalytic processes on these systems. Simultaneously, understanding the electronic structure that allows for the high activity, might aid the rational design of better catalysts for CO_2 activation.

Our results show that Cu(100) oxidizes from the pristine surface to a p(2×2) overlayer at 0.25 ML followed by a reconstruction to a $(2\sqrt{2} \times \sqrt{2})$R45° (MR) structure at 0.50 ML. Moreover, dissociative adsorption of CO_2 on Cu(100) occurs predominantly at surface steps. In_2O_3(110) is found to heavily hydroxylate in presence of H_2 and/or H_2O. Hydroxylation with H_2 causes the undercoordinated In-sites to change oxidation state (from In^{3+} to In^{2+}), while H_2O does not. We suggest that the redox capacity of the undercoordinated In-site are responsible for the adsorption of CO_2 on indium oxide, whereas oxygen vacancies act as spectators. Our results are in qualitative agreement with the experimental observation of heavy hydroxylation and the suppression of the reverse water gas shift on indium oxide.

Keywords: Heterogeneous catalysis, Density functional theory, Methanol conversion, CO_2 reduction, Copper surface, Indium oxide

En memoria de mis abuelos,
Salvador y Rosario y Feliciano y Lotero.
Que su recuerdo nunca me abandone.
Para mis papás.

List of Publications

This thesis is based on the following appended papers:

I. Initial oxidation of Cu(100) studied by X-ray photo-electron spectroscopy and density functional theory calculations
A. Posada-Borbón, B. Hagman, A. Schaefer, C. Zang, M. Shipilin,
A. Hellman, J. Gustafson and H. Grönbeck
Surface Science, **675** (2018), 64-69

II. Steps control the dissociation of CO_2 on Cu(100)
B. Hagman[‡], A. Posada-Borbón[‡], A. Schaefer, M. Shipilin, C. Zhang, L. Merte,
A. Hellman, E. Lundgren, H. Grönbeck and J. Gustafson
Journal of the American Chemical Society, **140** (2018), 12974-12979
[‡] Equal contribution

III. CO_2 adsorption on hydroxylated In_2O_3(110)
A. Posada-Borbón and H. Grönbeck
Submitted

Publications not included in the thesis:

Cluster Size Effects in Ethylene Hydrogenation over Palladium
A. Posada-Borbón, C.J. Heard and H. Grönbeck
The Journal of Physical Chemistry C, **121**(2017), 10870-10875

Correlation between ethylene adsorption energies and core-level shifts for Pd nanoclusters
A. A. Tal, A. Posada-Borbón, H.J. Grönbeck and I.A. Abrikosov
The Journal of Physical Chemistry C, **123**(2019), 2544-2548

My contributions to the publications

Paper I
I performed all the calculations and wrote the first draft of the paper, which was finalized together with my co-authors.

Paper II
I performed all the calculations and wrote the first draft of the theory section of the paper, which was finalized together with my co-authors.

Paper III
I performed all the calculations and wrote the first draft of the paper, which was finalized together with my co-author.

Contents

Chapter 1

Introduction

> "*... if we are to rely on alternative energy sources (biomass, solar or nuclear) and avoid serious environmental problems, we must develop new and improved solid catalysts"[1]*
>
> – Charles T. Campbell (2012)

There is a consensus in the scientific community that rapid climate change is linked to anthropogenic greenhouse-gas (GHG) emissions to the atmosphere [2–6]. In the assessment report of the Intergovernmental panel on climate change (IPCC), it is estimated that CO_2 amounted to at least 65% of all GHG emissions in 2010 $[7]^{p.7}$. Additionally, it is reported that ∼32% of all the GHG emission were produced by the industry $[7]^{p.9}$, out of which, one third were result of electricity and heat production $[7]^{p.752}$. Similarly, the consumption of energy for household usage and transportation, mostly dependent on fossil fuels, contributing with 26% to all emissions of GHG $[7]^{p.9}$. A detailed break down of GHG emissions is presented in Ref. [8], and a representative extract of it is shown in Figure 1.1. Given the multifactorial contributions to each sector, it is, nevertheless, hard to pinpoint the major source of greenhouse gas emissions. It is clear, however, that electricity and heat production combined with transport emissions amount to a significant portion of the total green house gas emitted to the atmosphere $[7]^{p.9}$. Hence, it is important to produce electricity and fuels for transportation that are environmentally friendly, if we are to reduce GHG emissions and to slow down rapid climate change.
Sweden is a good example of how this is possible on a national scale, given that 58 % of its electricity is produced from renewable sources $[9]^{p.7}$, whereas an impressive 90% of its electricity is produced without carbon emissions $[9]^{p.7}$. This is the result of nuclear power as a large source of Sweden's electricity. However, carbon-clean, nuclear power has other drawbacks, such as risk of great damage in case of malfunction and waste disposal issues. The last decades have seen a rapid technological development towards renewable energy sources. Among these, the recycling of greenhouse gases to added-value chemicals by

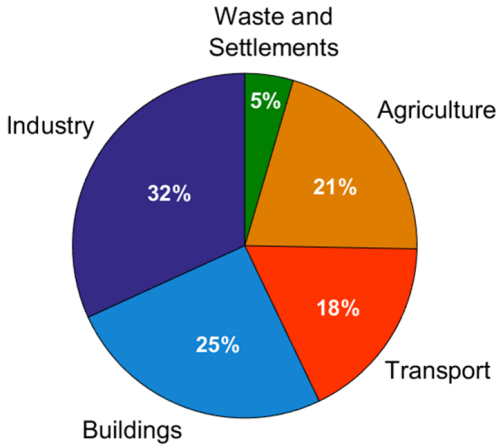

Figure 1.1: Greenhouse gas emissions by sector. Data taken from Ref. [8]).

catalytic conversion has been proposed as a possible way to reduce carbon emissions [10–18]. A promising pathway to depart from the current fossil-fuel dependence is the catalytic reduction of CO_2 to methanol (CH_3OH). This process has been proposed as a possible way to achieve a net zero sum of carbon emissions to the atmosphere, given that a closed-carbon loop can be attained. [10–15]. However, capture and storage of this green-house gas from the atmosphere is challenging. This issue can in some cases be circumvented by recapturing CO_2 directly from the plant exhaust.

One reason behind the strong fossil-fuel dependence is their high energy density. Diesel, gasoline and coal have have an energy density of 38, 34 and 27 MJ/l, respectively [19]. MeOH has an energy density of roughly half that of gasoline [20]. Additionally, methanol is liquid at room temperature, which make storage and transportation easy. Moreover, methanol can be combusted in gasoline engines, requiring only slight modifications. These reasons make it convenient as a renewable energy source. It should be noted that methanol not only is a possibly alternative fuel, it is also one of the largest primer feedstock chemicals [13]. Renewable production of methanol from captured CO_2 has been operational in large scale since 2012, in Iceland, at the "George Olah CO_2 to renewable methanol plant" in Svartsengi, Iceland [21].

CH_3OH is currently industrially produced, mostly, from synthesis gas (CO, CO_2 and H_2) which is obtained from natural, shale gas, and coal [13, 22]. This process is performed over a copper-based catalyst at relatively high temperatures and pressures (473 to 573 K,

5 to 10 MPa). This process is energy-intense, making large scale production necessary for the process to be efficient. This translates to methanol production requiring large processing plants where, for the most part, either natural gas or coal is used to produce syngas and MeOH. Furthermore, the copper-based catalyst faces many shortcomings, among them, rapid deactivation by sintering [23, 24].

It is evident that the production of renewable energy by catalytic conversion is challenging. Moreover, it is clear that longer-lasting and more cost-effective catalysts must be developed, if we expect methanol to be a feasible renewable energy source. It is the purpose of this thesis to contribute on the development of such materials.

1.1 Catalysis

Catalysis is the acceleration of a chemical reaction by a catalytic substance [25]. A catalytic substance, or catalyst, can be any sort of material or compound, as long as it makes the reaction occur faster than the uncatalyzed case and that it remains unchanged after the catalytic reaction. In a catalytic process, the catalyst allows for a kinetically unfavourable reaction path to take place by introducing a new pathway. In macroscopic terms, this is observed as a reduction of the activation energy for the reaction. It should be noted that a catalyst does not change the thermodynamics of a reaction, as the initial and final state of the overall process are the same as the ones for the uncatalyzed reaction. Thus, the change in the free energy in the reacting system is the same with or without catalyst [25, 26]. A schematic representation of this is shown in Figure 1.2.

A catalytic process is said to be heterogeneous when the catalyst and reactants are found in different aggregation state. If instead the reactants and catalyst have the same phase, the process is referred to be homogeneous[26]. A kind of biocatalytic process also exist, and refers to reactions performed by enzymes in biological systems [25, 26]. In this work we have focused on heterogeneous processes.

Reaction mechanisms on surfaces involve at least three elementary steps, namely, adsorption of the reactants, reaction at the surface and desorption of the products [25]$^{p.70}$. Moreover, reactions on surfaces can be broadly categorized depending on if all reactants adsorb at the surface or not. These are the *Eley-Rideal* and *Langmuir-Hinshelwood* mechanisms . These two surface reaction mechanisms are shown schematically in Figure 1.2. In the *Eley-Rideal* mechanism, one of the reactant species adsorbs at the surface.

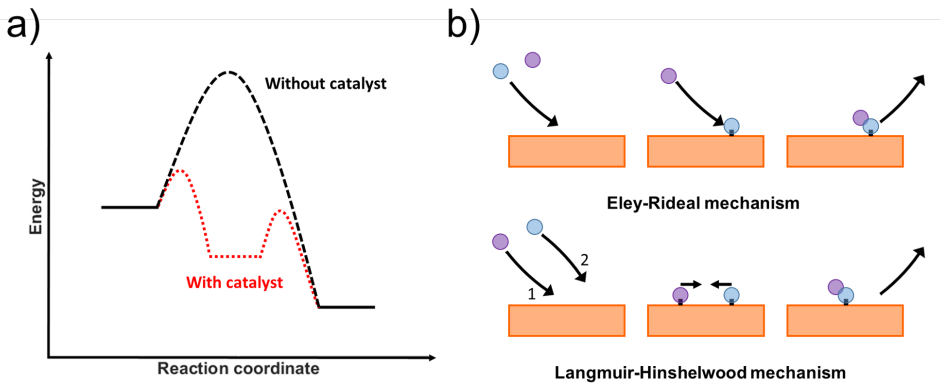

Figure 1.2: **Left:** Schematic sketch of a catalyzed and uncatalyzed chemical reaction. **Right:** Schematic illustration of two surface reaction mechanisms, *Eley-Rideal* (top) and *Langmuir-Hinshelwood* (bottom).

The reaction proceed as the second reactant reacts with the adsorbed species directly from the gas phase. Finally, the product desorbs from the surface leaving the catalyst surface unchanged. In the *Langmuir-Hinshelwood* mechanism, adsorption and reaction takes place at different times. As shown in the schematic in Figure 1.2, both reactants adsorb on the surface. This step is followed by diffusion of one or both of the adsorbates on the surface and ends with the adsorbates meeting and reacting on the surface forming a product. As in the first mechanism, desorption of the product leaves the surface unaltered. The *Langmuir-Hinshelwood* mechanism highlights a second important aspect of a heterogeneous catalyst, namely that it assembles the reactants and in this way facilitates the reactions. A third kind of mechanism, of particular importance for some redox reactions, is the *Mars-van Krevelen* mechanism [27]. This mechanism is characterized by the catalyst surface lattice donating one or more of its components to one of the products of the reaction [28]. For example, the creation of an oxygen vacancy in an oxide surface, which is replenished by another intermediate at a later step of the overall reaction mechanism [27].

Two important concepts that must be defined relating to catalysis are those of catalytic activity and catalytic selectivity. Price, availability and durability of a catalytic material, together with activity and selectivity, should also be considered for the rational design of a catalyst. Catalytic activity refers to the rate at which the reaction occurs, thus the number of products formed per unit time. Catalytic selectivity instead refers to the measure of the extent to which the catalyst produces the desired product. Both the activity and selectivity of a catalyst depend heavily on how strongly the reactants interact

with the catalyst. It is clear that a reactant should not bind too weakly with the catalyst as in that case it might desorb from the surface before the reaction takes place. Similarly, the reactants (or products) should not bind too strongly to the catalyst either, or the reaction can not take place (because of the catalyst being poisoned). The strength of interaction between a catalyst and the reactants/products needs to be a compromise. This idea was first proposed by french scientist Paul Sabatier, and its know as Sabatier's principle [25]. Finding a catalyst with a Sabatier compromise, which is also durable, economic and abundant, make rational catalyst design a challenging, but necessary, task.

Catalytic reactions are strongly dynamic, where the catalyst in some cases may change geometrically and chemically during the operation. Some experimental analysis techniques used to study catalytic reactions are based on spectroscopic methods, such as X-ray photo-electron spectroscopy, Infrared spectroscopy and Raman spectroscopy, that allow to study changes on the catalyst or the reactants (or both). Despite the wide repertoire of analysis techniques, sometimes understanding how and why a reaction occurs in the way it does on real catalysts, is too complicated. Hence, model systems (simplified structures to describe the catalyst and the reaction) are used to facilitate the understanding of the step-wise evolution of elementary reactions by which an overall chemical reaction takes place. Use of model systems is also used in theoretical research, and it is probably desirable to do so, as it keeps the convolution of interaction effects in the system limited to an extend we can comprehend. By providing understanding of the electronic structure of materials, we can help design effective catalysts that do not sinter or provide understanding on how and why some reaction mechanism are preferred on other materials.

One approach in heterogeneous catalysis to obtain information on surface reactions has been to study reactions over single crystal surfaces. This means the system can be studied with surface science tools, having atomic control over the surface and adsorbates [29].

1.2 Methanol conversion from CO_2 on Cu and In_2O_3

Methanol production by catalytic conversion of CO_2 is currently performed at high temperature and pressure (473-573 K, 5-10 MPa) with syn-gas over a Cu/ZnO/ Al_2O_3 catalysts [30–34]. Step sites have been suggested to be highly active for CO_2 activation on copper surfaces [33, 35, 36], however, the true nature of this site is debated [31]. Moreover, the copper catalyst is known to deactivate rapidly due to sintering [23, 24]. Additionally, hindering of CO_2 adsorption on copper has been linked to surface self-poisoning by surface

oxidation [34, 37, 38]. In response to this, research on catalysts capable of long-lasting hydroxylation of CO_2 to methanol has been active.

In recent years, an In_2O_3/ZrO_2 catalyst has attracted much attention, thanks to its high selectivity, activity and durability [39]. The durability of this catalyst has been linked to a hindering of sintering, which has been attributed to ZrO_2 [39]. Additionally, the high selectivity of In_2O_3 has been suggested, most predominantly in the experimental contribution of Bielz *et al.* [40], to be result of the suppression of the Reverse Water Gas Shift (RWGS) reaction [40–42]. Thus, CO is able to reduce In_2O_3, whereas, CO_2 is incapable of re-oxidizing the oxide [40].

A theoretical reaction mechanism has been proposed by Ye *et al.* [43] for the hydrogenation of CO_2 to CH_3OH on $In_2O_3(110)$. In this mechanism, the first step is the creation of an oxygen vacancy by hydrogen reduction of the surface. Subsequently, the mechanism proposes to quench the vacancy by CO_2 adsorption. The next step is the formation of formate (HCOO), followed by the formation of a dioxymethylene with a surface oxygen (H_2COO_{surf}), a methoxy (H_3CO) and finally methanol (H_3COH) [43, 44]. However, the quenching of the oxygen vacancy by CO_2 adsorption in this reaction mechanism appears to be in conflict with the experimental evidence of the suppression of the RWGS reaction [40]. Hence, determining the true role of oxygen vacancies at the surface is of high importance to understand why In_2O_3/ZrO_2 is active for CO_2 reduction to CH_3OH.

These conflicting results, both for copper and indium oxide, demonstrate that there is a need for systematic research on the conditions and reaction mechanisms under which reduction of CO_2 to methanol take place. In this thesis, we intend to explain what happens with copper in the early-stage oxidation process, upon which the adsorption of CO_2 has been reported to decrease [34]. Similarly, we intend to determine the effect of hydroxylation and the role of oxygen vacancies for the adsorption of CO_2 on $In_2O_3(110)$.

1.3 Aim of thesis

The aim of this thesis is to elucidate the process and thermodynamically stable surface conditions for activation and adsorption of CO_2 on copper and indium oxide. The understanding of this reaction step is of importance for catalyst design, as adsorption of CO_2 is the initial step for carbon dioxide reduction to methanol. In **paper I** and **II**, we study the oxidation process of Cu(100) and the dissociative-adsorption mechanism of

CO_2, respectively. This is done in a coupled theory/experiment approach. In particular, we make use of density functional theory (DFT) calculations in combination with ambient pressure x-ray photoelectron emission spectroscopy (AP-XPS) experiments to study CO_2 adsorption on Cu(100). In **paper III**, we study the nature and effect of hydroxylation on In_2O_3(110) with H_2 and H_2O. Additionally, the role of oxygen vacancies for CO_2 adsorption is investigated under pristine and hydroxylation conditions. Here, we make use solely of DFT calculations.

Density functional theory is discussed in detail in Chapter 2. The theoretical tools and AP-XPS, used for the characterization of surfaces and adsorbates, are presented and discussed in Chapter 3. Our results are presented in Chapter 4 and, lastly, the conclusions and outlook are presented in Chapter 5.

Chapter 2

Electronic structure calculations

> "*... It came out of the mind of Schrödinger (Schrödinger's equation), invented in his struggle to find an understanding of the experimental observation of the real world*"
>
> – R.P. Feynman *et al.*, 1965, chapter 16, p. 12.

Quantum mechanics describe how electrons interact and is the only way to unequivocally describe chemical reactions, like the activation of CO_2, which is achieved by the transfer of one electron from the surface to the molecule. However, analytic solution only exists for systems with one electron. Hence, computational/numerical methods are required to deal with atomic systems larger than the hydrogen atom.

2.1 Schrödinger's equation

One central equation in quantum mechanics is Schrödinger's equation (3.7). This is a first principles equation, which means it is based on fundamental physical concepts, without empirical parameters. This equation was presented by Erwin Schrödinger in 1926 as a formulation to describe electrons in the presence of an external potential (nuclei/electron interaction). Assuming a non-relativistic single electron system, where the potential interaction is time independent, the equation can be compactly written as,

$$\hat{H}\psi = E\psi \tag{2.1}$$

Here $\hat{H}$ is the Hamiltonian operator, which contains the energetic components to the system. ψ is the systems wavefunction, which entirely describe the system. E is the systems energy. It should be noted that the square of the norm of the wavefunction is a probability distribution function. This means that the integral of the product between the wave function and its complex conjugate over a determined region of space will be equal to the probability of finding the system in that region. For a single electron system

in a Coulomb potential (hydrogen atom), the Hamiltonian is written in atomic units[i] as,

$$\hat{H} = \hat{T} + \hat{V} = -\frac{1}{2}\nabla^2 - \frac{1}{r} \tag{2.2}$$

Where $\hat{T}$ is the kinetic operator and $\hat{V}$ is the potential energy term. This equation is slightly more complex for a system with N_n nuclei and N_e electrons [45],

$$\hat{H} = -\sum_I \frac{1}{2M_I}\nabla_I^2 - \frac{1}{2}\sum_i \nabla_i^2 - \sum_{i,I} \frac{Z_I}{|\mathbf{r}_i - \mathbf{R}_I|} + \sum_{\substack{i,j \\ j>i}} \frac{1}{|\mathbf{r}_i - \mathbf{r}_j|} + \sum_{\substack{I,J \\ J>I}} \frac{Z_I Z_J}{|\mathbf{R}_I - \mathbf{R}_J|} \tag{2.3}$$

Here, the first and second terms are the operator for the kinetic energy of the nuclei and electrons, respectively. The $\frac{Z_I}{|\mathbf{r}_i - \mathbf{R}_I|}$ sum refers to the electron-nuclei interaction and the sums run over all electrons and nuclei. Similarly, the $\frac{1}{|\mathbf{r}_i - \mathbf{r}_j|}$ sum is the electron-electron interaction. Lastly, the $\frac{Z_I Z_J}{|\mathbf{R}_I - \mathbf{R}_J|}$ term represents the electrostatic interaction between nuclei. Unfortunately, for a many-body system, equation (3.7) is too complicated to be solved. This means we have to make approximations to get an equation, or system of equations, that can be solves.

2.2 Born-Oppenheimer approximation

One common approximation made to simplify the many-body problem to a traceable set of equation is the assumption that the electronic and nuclei wave-functions can be decoupled. This is known as the Born-Oppenheimer (BO) approximation. The physical principle behind this approximation is that the nuclei are massive with respect to the electrons (the mass of the proton is 1836 times that of an electron) so that their movement in comparison to the one experienced by the electrons is negligible. Thus, the electrons are considered to adapt instantly to the movement of the nuclei [45].

If we consider a many-body system in the BO-approximation, we find that the total-system Hamiltonian can be split into electronic and nuclear components. This set of equations allows us to deal with the many-body problem in a two step fashion, by solving first the electronic Schrödinger equation in field of fixed nuclei and subsequently optimizing the nuclei geometry to minimize the energy of the system. The electronic Hamiltonian in

[i] In atomic units (a.u), the elementary charge (e), electron rest mass (m_e), Coulombs force constant ($k_e = \frac{1}{4\pi\epsilon_0}$) and Planck's reduced constant ($\hbar = \frac{h}{2\pi}$) are set to unity.

atomic units has the form,

$$\hat{H}_e = -\frac{1}{2}\sum_i \nabla_i^2 - \sum_{i,I} \frac{Z_I}{\mathbf{r}_{iI}} + \sum_{\substack{i,j \\ j>i}} \frac{1}{\mathbf{r}_{ij}} \tag{2.4}$$

Where the first term is the kinetic energy operator of the electrons. The second one is the Coulomb electron/nuclei interaction (from the fixed nuclei). The last term is the electron/electron repulsion.

The significance of the BO-approximation comes from the fact that, it makes it enough to solve the electronic configuration problem and to optimize iteratively the nuclei configuration and changes to the electronic states [46, 47]. Regardless of the simplification achieved by the use of the BO approximation, the many-electron system is still too complicated to work with. Thus, different methods have been developed over time to deal with this issue. These can be categorized into wave-function methods, based on Hartree-Fock [48, 49] and electronic density methods, like the Density Functional Theory (DFT) [50, 51]. It is not the purpose of this thesis to go in more detail on wave-function methods, which can be found elsewhere [45, 52].

2.3 Density functional theory

Density functional theory (DFT) is a quantum mechanical formulation for the description of many-body systems that relates the total energy of the system with the electron density. Attempts to use the electronic density as the central variable have been presented earlier in the Thomas-Fermi model [53, 54], but had been found unable to properly describe chemical bonds.

The working principle behind DFT is that the electronic density of a system can be used to exactly describe its ground state energy. This is achieved by expressing the ground state energy of the system as a functional of its electronic density. Within the Kohn-Sham approximation, the energy is obtained by solving a *Schrödinger-like* set of equations in a variational minimization approach. DFT is, in principle, an exact quantum mechanical theory, that within the Kohn-Sham approach, manages to decompose a many-interacting-electron equation into many non-interacting single electron equations.

2.3.1 Hohenberg and Kohn: Electronic density

The seminal work of Pierre Hohenberg and Walter Kohn [50] (HK) lays the foundation upon which density functional theory is built on. HK successfully show in their work that the electronic density of the ground state, n($\mathbf{r}$), of an interacting electron system in an external potential $V_{ext}(\mathbf{r})$ uniquely determines the potential, up to an additive constant. This implies that the Hamiltonian is described at the ground state uniquely by the ground state electronic density and it is, by consequence, a functional of it. Moreover, HK show that the energy of a system is described by a universal functional of the electronic density F[$n(\mathbf{r})$]. This is explicitly written as,

$$E\left[n(\mathbf{r})\right] = \int V(\mathbf{r})n(\mathbf{r})d\mathbf{r} + F\left[n(\mathbf{r})\right] \tag{2.5}$$

Where, for the correct electronic density, E[$n(\mathbf{r})$] becomes the ground state energy of the system. Additionally, it is convenient to separate Coulomb long-range interactions from the functional F[$n(\mathbf{r})$],

$$F[n(\mathbf{r})] = \frac{1}{2}\int\int \frac{n\left(\mathbf{r}\right)n\left(\mathbf{r}'\right)}{|\mathbf{r}-\mathbf{r}'|}d\mathbf{r}d\mathbf{r}' + G\left[n\left(r\right)\right] \tag{2.6}$$

and to rewrite the energy functional term as,

$$E\left[n(\mathbf{r})\right] = \int V(\mathbf{r})n(\mathbf{r})d\mathbf{r} + \frac{1}{2}\int\int \frac{n\left(\mathbf{r}\right)n\left(\mathbf{r}'\right)}{|\mathbf{r}-\mathbf{r}'|}d\mathbf{r}d\mathbf{r}' + G\left[n\left(\mathbf{r}\right)\right] \tag{2.7}$$

Where the first term is the energy contribution by the external potential. The double integral is the classical electron-electron interaction (Hartree) to the energy of the system and G[$n\left(\mathbf{r}\right)$] is a universal functional of the electronic density, which conveniently encloses kinetic energy and all the quantum mechanical effects. The exact form of G[$n\left(\mathbf{r}\right)$] is, however, unknown. The work of HK successfully replaces the many-body wave function with the electronic density as the main incognita in quantum mechanical systems.

2.3.2 Kohn and Sham: Kohn-Sham equations

One year later, in 1965, Walter Kohn and Lu Sham [51] provided an approximation to the universal G[$n\left(\mathbf{r}\right)$] functional. This was done by replacing the interacting-electron system with a system of non-interacting electrons. This allows to approximate the systems kinetic energy with a correct description for this term and leads to the Kohn-Sham equations, a set of Schrödinger-like equations, that describe the electronic system as a set of single particle equations in an effective potential.

The assumption that the interacting electrons can be described as a non-interacting system allows to write the universal functional as,

$$G\left[n\left(\mathbf{r}\right)\right] = T_S\left[n\left(\mathbf{r}\right)\right] + E_{xc}\left[n\left(\mathbf{r}\right)\right] \tag{2.8}$$

where T_S is the kinetic energy of the non-interacting system and E_{xc} is the exchange-correlation functional. The E_{xc} functional can be approximated in different ways and encloses all the quantum mechanical effects on DFT. The kinetic energy of the non-interacting system can be described by single-electron determinant wavefunctions, such that the kinetic energy of the non-interacting system is given as,

$$T_S\left[\left(\mathbf{r}\right)\right] = -\frac{1}{2}\sum_i \left\langle \phi_i \right| \nabla^2 \left| \phi_i \right\rangle \tag{2.9}$$

The density is given in term of the single-electron Kohn-Sham orbitals (ϕ_i) as,

$$n\left[\left(\mathbf{r}\right)\right] = \sum_i \left|\phi_i\left(\mathbf{r}\right)\right|^2 \tag{2.10}$$

The exchange-correlations functional is explicitly written as,

$$E_{xc}\left[n\left(\mathbf{r}\right)\right] = \left(T\left[n\left(\mathbf{r}\right)\right] - T_S\left[n\left(\mathbf{r}\right)\right]\right) - \left(V_{int}\left[n\left(\mathbf{r}\right)\right] - J\left[n\left(\mathbf{r}\right)\right]\right) \tag{2.11}$$

Here, $\mathrm{T}[n\left(\mathbf{r}\right)]$ and $\mathrm{T}_S\left[n\left(\mathbf{r}\right)\right]$ are the kinetic energy of the interacting and non-interacting electron system, respectively. $V_{int}[n\left(\mathbf{r}\right)]$ is the total electron-electron interaction (see equation (2.3)) while $J[n\left(\mathbf{r}\right)]$ is the classical Coulomb electron interaction. $\mathrm{E}_{xc}\left[n\left(\mathbf{r}\right)\right]$ takes into account the fermions antisymmetric nature of the electrons as well as the non-classical electron-electron correlation [55]. The total energy functional of the interacting system is given by,

$$E\left[n(\mathbf{r})\right] = \int V_{ext}(\mathbf{r}) n(\mathbf{r}) d\mathbf{r} + \frac{1}{2}\int\int \frac{n\left(\mathbf{r}\right) n\left(\mathbf{r}'\right)}{\left|\mathbf{r}-\mathbf{r}'\right|} d\mathbf{r} d\mathbf{r}' + T_S\left[n\left(\mathbf{r}\right)\right] + E_{xc}\left[n\left(\mathbf{r}\right)\right] \tag{2.12}$$

Where minimization of the energy functional with respect to the density assures that the density is that of the ground state. From a Lagrange-multiplier procedure, and given that the total number of electrons remains constant N, we can derive the Kohn-Sham (KS)

equations for the i electron in an effective potential, expressed as,

$$\left[-\frac{1}{2}\nabla_i^2 + v_{eff}\left(\mathbf{r}\right)\right]\phi_i = \epsilon_i\phi_i \tag{2.13}$$

The significance of this equation is that it allow us to go from an unsolvable many-electron equation, to a set of coupled single-electron equations. The effective potential is given as,

$$v_{eff}\left(\mathbf{r}\right) = V\left(\mathbf{r}\right) + v_{xc} + \int \frac{n\left(\mathbf{r}'\right)}{\left|\mathbf{r}-\mathbf{r}'\right|} d\mathbf{r}' \tag{2.14}$$

$$v_{xc} = \frac{\partial E_{xc}}{\partial n\left(\mathbf{r}\right)} \tag{2.15}$$

Where v_{xc} is the exchange-correlation potential, and the total energy of the system is given in terms of the Kohn-Sham eigenvalues ϵ_i as,

$$E = \sum_i \epsilon_i + E_H + E_{xc} - \int n\left(\mathbf{r}\right) v_{xc}\left(\mathbf{r}\right) d\mathbf{r} \tag{2.16}$$

To determine the total energy of the system, the KS equations are solved in a self-consistent fashion, where the single-electron equations are solved iteratively from an initial guess density. For the exact exchange-correlation functional, the highest occupied eigenvalue would be equal to the negative of the ionization energy. This is known as Janak's theorem [56], where the derivative of the total energy with respect to the occupation of an orbital equals the specific KS eigenvalue of that orbital [56]. However, as they represent the non-interacting system, the Kohn-Sham eigenvalues have no direct physical meaning.

2.3.3 Exchange-correlation functionals and Jacob's ladder

One should notice the magnitude of the contributions of the different terms in equation (2.12). In ref. [57], it is shown that for the values of a Mn atom, the most dominant term is the electrostatic interaction between the core and the valence electrons, followed by the electronic kinetic energy of the non-interacting electrons, with the electrostatic interaction between the valence electrons in a third place and exchange-correlation energy being the smallest term. However, the significance of the exchange-correlation term is clearly exemplified in Ref. [58], where it is shown that without this term atomization energies are massively underestimated. A similar trend is found for surface energies and work functions [58]. It is the exchange-correlation term that accounts, to the greatest extend, for chemical bonds. Without the exchange-correlation term, the Kohn-Sham equations

can be reduce to a reformulation of Hartree-Fock equations without exchange [59]. The exact expression of the exchange-correlation term is unknown and has to be approximated.

Different approximations have been proposed to describe the exchange-correlation functional. Typically, the precision with which the term is described is improved by increasing the detail with which the functional depends on the electronic density. These approximations have been ordered in the so called *Jacobs-ladder* described by Perdew and Schmidt [59], a schematic representation of this is shown in Figure 2.1.

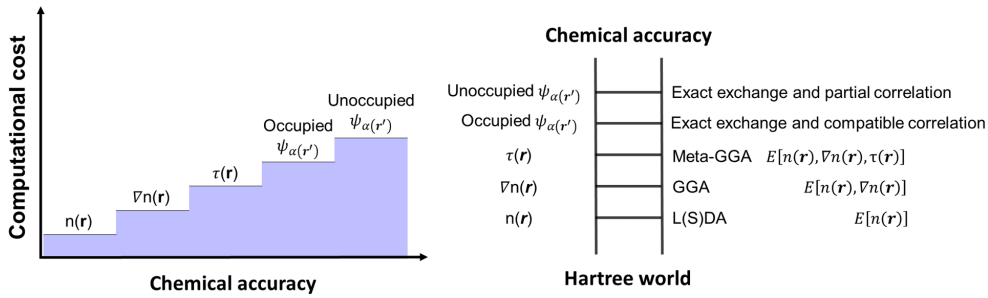

Figure 2.1: **Left:** Schematic view of the computational cost as a function of chemical accuracy (own). **Right:** Schematic depiction *Jacob's ladder* adapted from Ref [59]

Given that all steps in Jacobs ladder are approximations, the actual *accuracy* will depend on whether the chosen functional approximation describes the nature of the system. This means that there is no guarantee that using a functional on a higher rung in the ladder will produce a better description of a system. Only the exact exchange-correlation functional would guarantee chemical accuracy for any system.

Local Density Approximation

The simplest of the approximations to the E_{xc} functional is the one made by Kohn and Sham themselves [51], where the exchange-correlation functional is approximated only as a functional of the electronic density of an homogeneous electron gas. This is expressed as,

$$E_{xc}\left[n\left(\mathbf{r}\right)\right] = \int n\left(\mathbf{r}\right) \epsilon_{xc}^{hom}\left(n\left(\mathbf{r}\right)\right) d\mathbf{r} \tag{2.17}$$

where $\epsilon_{xc}^{hom}\left(n\left(\mathbf{r}\right)\right)$ is the exchange-correlation energy per electron in the homogeneous non-interacting electron system of density $n(\mathbf{r})$. This approximation can be easily generalized

to include spin component by considering the electron gas to have uniform spin densities, $n_{\uparrow}(\mathbf{r})$ and $n_{\downarrow}(\mathbf{r})$. The expression has in this case a spin dependence, giving also the KS orbitals a spin-dependence. The LDA approximation can reproduce trends for extended systems, where the electronic density changes slowly. However it is known to underestimate bond-lengths and to overestimate binding energies [57]. Moreover, given the local character of the electronic density, L(S)DA is poor at describing band-gaps in oxides, and in describing molecules.

Generalized Gradient Approximation

Attempts at correcting for the shortcomings of LDA and describe a non-uniform but slowly changing density is done by including an inhomogeneity dependence of the exchange-correlation functional on the density. This is done in the Generalized Gradient Approximation (GGA), where the exchange-correlation functional depends on the density and its gradient, $\mathrm{E}_{xc}[n(\mathbf{r}), \nabla n(\mathbf{r})]$.

A good example of these approximation is the one done by Perdew, Burke and Ernzerhof [60], in the, so-called, PBE-functional. This functional is constructed to fall back to LDA in the limit of the uniform electron gas [60], recovering in this way all the exact xc-hole constraints [60, 61]. GGA functionals have an E_{xc} functional of the form,

$$E_{xc}[n(\mathbf{r})] = \int n(\mathbf{r})\, \epsilon_{xc}^{hom}(n(\mathbf{r}))\, F_{xc}[n(\mathbf{r}), \nabla n(\mathbf{r})]\, d\mathbf{r} \tag{2.18}$$

Here, F_{xc} is an enhancement factor that modifies the LDA energy [60]. GGA's of this family are know to better describe bond-lengths than LDA, but are also known to underestimate binding energies and fail to describe strongly-correlated systems [62]. Further refinements can be done to the exchange-correlation functional and one example is meta-GGA's, where the E_{xc} is also made a function of kinetic energy of the electronic density $\mathrm{E}_{xc}[n(\mathbf{r}), \nabla n(\mathbf{r}), \tau(\mathbf{r})]$.

Hybrid functionals

An additional level on Jacob's ladder for exchange-correlation functionals comes when including an exact exchange term, calculated as for Hartree-Fock with the use of KS orbitals [59]. This possibility was first explored by Becke [63], using the Parr-Wang functional as a basis [64]. The exchange integral in Hartree-Fock and the exact exchange have the form,

$$K_{ij} = \int \phi_i^* (\mathbf{r}) \, \phi_j (\mathbf{r}) \, \frac{1}{|\mathbf{r} - \mathbf{r}'|} \phi_i (\mathbf{r}') \, \phi_j^* (\mathbf{r}') \, d\mathbf{r} d\mathbf{r}' \tag{2.19}$$

$$E_x^{exact} = -\frac{1}{2} \sum_{i,j}^{occ} K_{ij} \tag{2.20}$$

The exchange-correlation functional for a hybrid functional can be written as,

$$E_{xc}^{hybrid} = E_{xc}^{GGA} + \alpha \left(E_x^{exact} - E_x^{GGA} \right) \tag{2.21}$$

where factor α is a mixing parameter, usually taken as $\alpha = 0.25$. Hybrid functionals tend to exhibit good behavior for systems with localized densities, such as metal oxides [65]. These kind of systems tend to be described poorly by LDA and GGA functionals, due to issues with the self-interaction energy, which is not entirely canceled in the lower rungs of Jacob's ladder [65]. However, exactly evaluating the exchange term over all orbitals comes at a cost, and hybrid functionals are far more computationally intensive than LDA or GGA [65].

Effects of van der Waals

van der Waals forces are the result of fluctuating dipole interactions [66]. This induces dynamical long-range attractive interaction between otherwise non-interacting atoms. These interactions are part of the exact exchange-correlation functional, however, they are not properly accounted for in LDA, GGA or hybrid functionals. It is customary to include this energetic contribution as a correction to the Kohn-Sham energy. This is the case for the Tkatchenko-Scheffler [67] or the Grimme D2/D3 [68, 69] methods. An exchange-correlation functional that attempts to account for van der Waals interactions is the Chalmers-Rutgers (vdW-DF-cx) [66]. van der Waals interactions are in particular important when investigating interactions between closed-shell systems.

2.3.4 Basis sets

The Kohn-Sham orbitals, ϕ_i, need to be represented and in most applications they are expanded in a basis as,

$$\phi_i = \sum_{\alpha} C_{\alpha i} G_{\alpha} \tag{2.22}$$

Where G_α can be expressed as atomic-orbital-like functions and the sum takes over the number used basis functions. In this way, the Kohn-Sham orbitals are represented a linear

combination of atomic-orbitals centered on the atoms [52]$^{p.442}$. This representation is useful in understanding chemical bonding in molecular systems, as the bond is result of the overlap of the atomic orbitals of each atom. This a powerful technique, that makes electronic structure and bonding intuitive, but its accuracy depends very strongly on the chosen basis set. The atomic orbitals can take the form,

$$G_\alpha = S^\zeta_{\alpha,nlm}(r,\Theta,\phi) = Nr^{n-1}e^{-\zeta r}Y^m_l(\Theta,\phi) \tag{2.23}$$

$$G_\alpha = \phi_\alpha(x,y,z;\gamma,i,j,k) = Nx^i y^j z^k e^{-\gamma\left(x^2+y^2+z^2\right)} \tag{2.24}$$

Where the equation (2.23) is an expression for Slater type orbitals, while equation (2.24) is for Gaussian type orbitals [52]$^{p.442}$. The basis sets, however, can also be expressed as a sum of plane waves, which is a convenient expression for extended-periodic systems [70].

Plane waves

Implementation of the Kohn-Sham approach with plane-waves often use Bloch's theorem[70], which comes from considering a single electron moving in a periodic potential, where the periodicity of the external potential reproduces that of the Bravais lattice of a given crystal system [70]. Here, the wavefunction can be expressed as [71]$^{p.133}$,

$$\psi_{n\mathbf{k}}(\mathbf{r}) = e^{i\mathbf{k}\cdot\mathbf{r}}u_{n\mathbf{k}}(\mathbf{r}) = \sum_{\mathbf{G}} C_{n,\mathbf{k}+\mathbf{G}}e^{i(\mathbf{k}+\mathbf{G})\cdot\mathbf{r}} \tag{2.25}$$

Where the exponential term is a plane wave with wavevector $\mathbf{k}$, in the electronic band n within the first Brillouin zone (The Wigner-Seitz primitive cell of the reciprocal lattice[71]$^{p.89}$), and the $\mathrm{u}_{n\mathbf{k}}(\mathbf{r})$ represents a function with the lattice periodicity [72]$^{p.20}$. The assumption is that it is enough to describe the electrons within the first Brillouin zone while enforcing the lattice periodicity [71]$^{(p.129-130)}$. In principle, an infinite number of k-vectors are needed to describe the electronic structure of a system. In practice, a cut-off to the number of wavevectors included in the eigenfunctions is determined as,

$$\frac{1}{2}|\mathbf{k}+\mathbf{G}|^2 < E_{cut} \tag{2.26}$$

Where $\mathbf{k}$ are the wavewectors and $\mathbf{G}$ are the reciprocal lattice vectors.

Brillouin zone sampling

In k-space, the integrals that arise from solving the KS equation are described as sums. Given that it is sufficient to describe only the propagation over the first Brillouin zone (BZ), it is enough to evaluate this sums over some points of the BZ. The way in which the number and distribution of points is generated is diverse [73, 74]. In this work we have used Monkhorst-Pack scheme for k-point sampling [73]. This means that a grid of ($\mathrm{R}_a \times \mathrm{R}_b \times \mathrm{R}_c$) generates a uniform distribution of k-points as [73],

$$k_{a,b,c} = u_a \cdot \mathbf{b}_1 + u_b \cdot \mathbf{b}_2 + u_c \cdot \mathbf{b}_3 \tag{2.27}$$

$$u_a = \frac{2r - q_r - 1}{2q_r};\ r = [1, 2, ..., q_r] \tag{2.28}$$

where, $\mathbf{b}_i$ are the primitive reciprocal lattice vectors and q_r is the number of k-points in the a-direction.

Projector Augmented Waves Method

An approximation that is usually made for the description of atoms with DFT is that the core and semi-core electrons are treated as frozen. This means that the core states are viewed as identical to the atomic core states [75]. This is done to reduce computational cost, and is justified by the inactivity of core electrons in chemical bonding [76]. Additionaly, this method allows to efficiently compute DFT densities expressed in plane-wave basis sets.

The projector augmented wave method [76] (PAW) is an all-electron method that facilitates computation of plane wave-based wavefunctions in DFT. The PAW method splits the atomic-centered wavefunction into separate regions. Near the valence, where the wave function is usually smooth and well-behaved, and near the core, where the wave function oscillates rapidly due to the othorgonality constraint [76]. In the PAW approach, the rapidly oscillating wavefunction is replaced, through a transformation operator τ, into a smooth pseudo-wavefunction (PS). Similarly, the valence part is transformed into an envelop function [76], described also by an auxiliary function and the transformation operator.

Under this approach, it is possible to define the functional for the total energy in term of

these auxiliary wavefunctions and the transformation operator as [76],

$$\frac{\partial E\left[\tau\left|\tilde{\psi}\right\rangle\right]}{\partial\left\langle\tilde{\psi}\right|} = \epsilon\tau^{\dagger}\tau\left|\tilde{\psi}\right\rangle \tag{2.29}$$

Where $\tilde{\psi}$ are the auxiliary wavefunctions. These are in turn expressed in terms of a linear combination of partial wave functions. In this way, it is possible to describe the all-electron wave function as a linear combination of these auxiliary, both valence and pseudo, wavefunctions as,

$$|\psi\rangle = |\tilde{\psi}\rangle + \sum_{i}\left(|\phi_i\rangle - |\tilde{\phi}_i\rangle\right)\langle\tilde{p}_i|\tilde{\psi}\rangle \tag{2.30}$$

Where ϕ_i and $\tilde{\phi}_i$ are the all-electron partial wavefunction and partial pseudo-wavefunction, respectively. While, $\tilde{p}_i$ is a projector function. It is important to notice that the wavefunctions are well behaved all over the space they are defined on and are smooth at the boundary.

2.3.5 Self-consistency algorithm

The self-consistency algorithm followed in Kohn-Sham implementation is shown in Figure 2.1. The scheme begins by proposing an initial electronic density, usually a superposition of atomic densities. From this, we evaluate the KS effective potential, as stated in equation 2.14. Then we proceed to solve the KS equation in a self-consistent fashion, until a criteria on total energy change is achieve (SCF loop). If the change in density is below a convergence criteria, we proceed to calculate the total energy and forces.

The forces on the atom evaluated with a converged density from the SCF-loop can be used to optimize the atomic structure of the system.

2.4 Local energy minima

The structural minimization of an atomic system to its local minimum is an important part in the study of atomic structures and in the study of surface reactions. The physical justification for this comes from statistical mechanics, as in nature, an atomic structure will spend a majority of their time in the ground state energy minima. This is a minimization mathematical problem, and given the electrostatic nature of the nuclei/nuclei

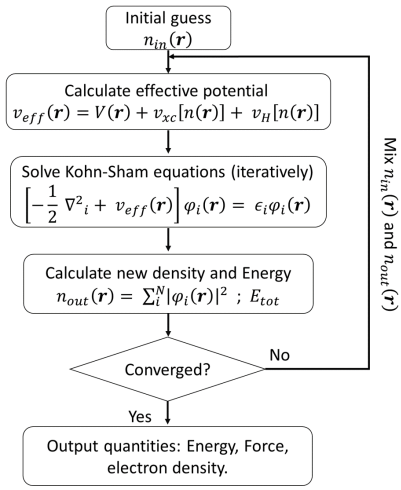

Figure 2.2: Self-consistency algorithm for DFT-calculations.

interaction, geometrical optimization is simply the minimization of atomic forces[ii]

There are many different algorithms that have been developed for the geometrical optimization of atomic structures [75]. Some of these algorithms are, RMM-DIIS, LBFGS, steepest decent and conjugate gradient. In this thesis, we have used the conjugate gradient algorithm. The basic principle behind conjugate gradient minimization is that after the first step (following the steepest descent) the next steps preserve the minimization made in the previous steps and only adds conjugate variations [75].

Finding the minimum energy structure of a system corresponds to finding a local minimum in its potential energy hypersurface (PES). The PES is a 3N dimensional object in a 3N+1 dimensional space, where N is the number of atoms in the system and the extra dimension is the value of the potential energy function [46]$^{p.4}$. Rotational and translational invariance in the system reduce the number of dimensions that described the PES. For diatomic molecules, the potential energy is entirely described by the interatomic distance [46]$^{p.123}$.

[ii] In a conservative field, the force acting upon a system is negatively proportional to the gradient of the potential energy of the system ($f_i = -\frac{\partial E}{\partial R_i}$)

2.5 Transition states and energy barriers

Another point of interest in the PES are the transition states, which correspond to saddle points in the immediate neighborhood between two local minimum energy basins. For a chemical reaction, the transition state is the lowest laying saddle point between the reactant and product minima. A limiting aspect on the search for transition states is that the saddle point is a minima in all but one directions [77]. Because of this, computational methods have been developed to aid in the search of these points. One such method, used in this thesis, is the nudged elastic band method [77].

Nudged Elastic Band

In the nudged elastic band method, an interpolation of structures (images) is constructed between the initial and final states of a chemical reaction. The images are kept together at equal distance from each other through the use of spring forces. A minimization on the overall force between these images, coming from both the system and the spring, drives the reaction pathway to a minimum energy path in the PES [77]. The force to minimize on each image is,

$$F_i = kR - \nabla E\left(\mathbf{R}_i\right)|_{\perp} \tag{2.31}$$

Where, the kR term corresponds to the force of the springs that connects the image with the one ahead, and the one behind. $\nabla E\left(\mathbf{R}_i\right)|_{\perp}$ is the perpendicular component of the total force of the image. Hence, a minimization on this force means that the local minimization of the images is guaranteed, while the minimization on the spring term should eventually converge to a minimum energy path [77]. An extension on this method is the introduction of the *climbing image* technique, where the maximum energy image is dragged to the top of the band relaxation by maximizing the perpendicular component of the total force experienced by that image and by releasing the image from its springs. This guarantees that the image will move upwards in the PES while remaining in the MEP. An example of the main reaction intermediates in the MEP found for CO_2 dissociation on Cu(100) is shown in Figure 2.3, as in **Paper II**.

A way of corroborating if we have found a true saddle point in the MEP connecting two local minima is to calculate the normal vibrational modes. A true saddle point will have one imaginary frequency in the direction parallel to the reaction coordinate. There might be more than one imaginary frequency if the PES is branching to different final states.

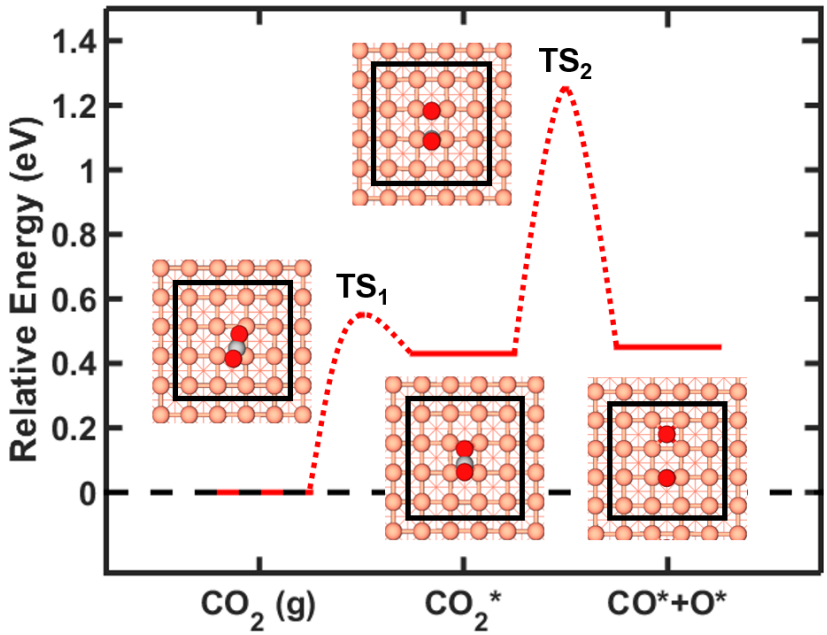

Figure 2.3: Reaction intermediates of CO_2 dissociation of Cu(100). Transition states are found with CI-NEB and corroborated with vibrational analysis.

2.6 Vibrational analysis

A way of determining the nature of points in the PES can be done by calculating its vibrational normal modes. This is done in the harmonic approximation and the forces acting upon the system are calculated as the derivative of the assumed harmonic potential. This effectively means that the forces are calculated by finite differences. In this procedure, the frequencies are obtained by diagonalizing the Hessian matrix, which describe the local curvature of the PES. The terms of the Hessian are second order derivatives to the potential energy, of the form $\frac{\partial^2 f(x_i,x_j)}{\partial x_i \partial x_j}$. The normal-mode frequencies are calculated as $\nu_i = \frac{1}{2\pi}\sqrt{\epsilon_i}$, where ϵ_i are the eigenvalues to the diagonalization of the Hessian matrix [78]$^{p.527}$. A negative eigenvalue term in the Hessian means a saddle point of the energy function in that frequency mode.

The vibrational frequencies can also be used to approximate molecular entropy (in the harmonic approximation). The vibrational component of the entropy is the significant contribution for strongly bound adsorbates. The frequencies are also used to determine a

systems zero point energy (ZPE) ($E_{ZPE} = \frac{1}{2}\hbar w_i$).

It is remarkable how many different aspects of molecular interaction can be tended to by a relatively simple approximation, as the harmonic oscillation for molecular systems. The accuracy of this approximation, however, relies deeply on the accurate description of the atomic interactions in a system. DFT provides a powerful machinery for this purpose. Being exact in principle, it allows for electronic structure calculations to be utilized, under a range of approximations, to describe somewhat accurately atomic processes such as heterogeneous catalysis. In this thesis, we have used the machinery of DFT and thermodynamics, along with ambient pressure XPS to determine the stability of surface structures and molecular dissociative-adsorption of CO_2 on Cu(100) and In_2O_3(110).

Chapter 3

Characterization of surfaces and adsorbates

"*... In this house we obey the laws of thermodynamics!*"

– Homer Simpson

Density functional theory calculations have evolved to a state where accurate description of materials and chemical interactions are possible. DFT predictions of experimental measurements can be made both regarding the state of the catalyst during reaction conditions and on the nature of the adsorbates. A coupled theory-experiment approach allows for a comprehensive understanding of catalytic reactions. This understanding is important when trying to determine the active site and reaction pathway for reactions.

One example of a method that is used to analyze the state of the catalyst during reaction conditions is *ab initio* thermodynamics. *ab initio* thermodynamics connects DFT calculations with thermodynamics by considering that the system is in equilibrium with reservoirs of the species it contains. In this way, thermodynamic contributions to the zero-temperature DFT calculations and predictions at experimental conditions can be made. In this thesis, we make use of *ab initio* thermodynamics predictions in **paper I** and **paper III** to determine the stable surface structure at experimental conditions. Another method we use to connect to experimental XPS measurements, is to calculate core level shifts (CLS).

DFT calculations provide access to the ground state electron density and the Kohn-Sham orbitals together with its eigenvalues. Analysis of the electronic structure is important in attaining understanding the chemical bonds in the system. The techniques for electronic structure analysis we have used are Bader charge analysis (BCA) and analysis of the Density of States (DOS). BCA allows for the analysis of charge localization in the system. This can be useful to determine reaction induced charge exchange. DOS analysis is

the investigation of the eigenvalue spectrum. The combined use of electronic structure analysis and computation of experimental observables can be useful to provide chemical understanding of reactions and surfaces. For example, CLS and BCA can be used together to determine the change in core-electron binding energy and the charge localization (oxidation state) on the system, respectively.

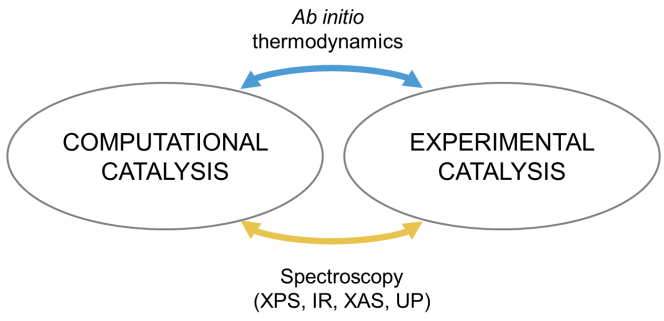

Figure 3.1: Relation between computational and experimental catalysis.

3.1 Ab initio thermodynamics

Density functional theory calculations are capable of describing chemical bonds. However, zero kelvin DFT calculations represent the system far from ambient conditions and usually do not account for thermodynamic contributions. However, thermodynamic contributions can be introduced separately, to account for temperature and pressure effects. This is done using the formalism of *ab initio* thermodynamics [79, 80].

The working principle behind *ab initio* thermodynamics is that an atomic system in thermodynamic equilibrium with its environment can be described in terms of thermodynamic variables [79, 80]. In this way, the thermodynamically preferred state of the system can be predicted. We notice that the formalism follows a kind of zeroth law of thermodynamics, meaning that when a system that is composed of subsystems is in equilibrium, then the subsystems are in equilibrium between themselves. These considerations allow us to describe surfaces, like Cu(100) or $In_2O_3(110)$, in a chemical environment, with, for example, O_2, H_2 or H_2O pressures. The surface free energy for any surface is written as,

$$\gamma\left(T, p_i\right) = \frac{1}{A}\left[G_{surf} - \sum_i N_i \mu_i\left(T, p_i\right)\right] \tag{3.1}$$

where A is the area of the surface cell, G_{surf} is the Gibbs free energy of the surface system and μ_i is the chemical potential of the atomic species considered in the system. The surface Gibbs free energy has the form,

$$G_{surf} = E^{tot} + E^{ZPE} - TS^{vib} - TS^{conf} + pV \tag{3.2}$$

Where E^{tot} is the adsorbate/surface system total energy, E^{ZPE} is the zero point energy, S^{vib} is the entropy vibrational contributions to the system which might be neglected if the contributions from the adsorbates are small, S^{conf} is the configurational entropy and pV is a pressure times volume term experienced on the surface-cell. The last term is, in practice, neglected because of the small volume in the surface-cell. In our approximations, we neglect the vibrational contributions from the lattice and configurational entropy.

In the case of surface reconstructions, we assume that the bulk structure acts as a reservoir of surface atoms, and we calculate the species chemical potential (μ_i) as the cohesive energy. In the case of adsorbates, like O_2, H_2 or H_2O, μ_i is calculated with respect to a gas phase ideal gas reservoir. The chemical potential of oxygen as the explicit form of,

$$\mu_O(T,p) = \frac{1}{2}\left[E_{O_2} + E^{ZPE}_{O_2} + \mu'_{O_2}(T,p_0) + k_B T ln\left(\frac{p_{O_2}}{p^0}\right)\right] \tag{3.3}$$

Where the factor of a half comes from the fact that the chemical potential is expressed in terms of an O_2 molecule. The first term (E_{O_2}) is the total energy of the O_2 molecule. $E^{ZPE}_{O_2}$ is the zero point energy of O_2, which we neglect. $\mu^{'}_{O_2}(T,p_0)$ is the reference chemical potential and the last term is the O_2 partial pressure contributions to the oxygen chemical potential. The $\mu^{'}_{O_2}(T,p_0)$ term is calculated from standard value pressures of enthalpy and entropy from thermodynamic tables [81] as defined in Ref. [79] as,

$$\mu'_{O_2} = \Delta H - T\Delta S; \tag{3.4}$$

$$\Delta H = H(T,p_0) - H(0,p_0); \tag{3.5}$$

$$\Delta S = S(T,p_0) - S(0,p_0); \tag{3.6}$$

In **paper III**, the chemical potential of H_2 and H_2O are calculated in the same way, and are ZPE corrected. A reference system is needed to evaluate how the surface free energy changes upon an species adsorption. In **paper I** we use the corresponding pristine surface a reference. In **paper III** we used the term ΔG^{ads}(T,p) instead of γ (T,p) to make it clear that we consider the adsorbates vibrational entropy and ZPE energy contributions

explicitly. This leads to a change in surface free energy of the form,

$$\Delta G^{ads}\left(T,p\right)=\frac{1}{A}\Big[\left(E_{ads/surf}+N_{ads}\left(E_{ads}^{ZPE}-TS_{ads}^{vib}\right)\right)-E_{surf}-N_{ads}\mu_{ads}(T,p)\Big] \tag{3.7}$$

The suffix *ads* is used to denote either H_2 or H_2O in **paper III**. It is important to note that all energies in Eq. (3.7), expect for the $\mu_{O_2}^{'}\left(T,p_0\right)$ term, are the result of DFT calculations. The formalism of *ab initio* thermodynamics provides a way of bridging between electronic structure calculations and macroscopic measurable systems at experimental pressure conditions.

3.2 X-ray spectroscopy

A common method used for the chemical characterization of materials is X-ray photoelectron spectroscopy (XPS). This experimental technique is also known as electron spectroscopy for chemical analysis (ESCA), which is the name given by Kai Seigbahn, that highlights that the technique can be used for chemical analysis. The core-level shifts (CLS) can be calculated using DFT. Both experimental and theoretical methods were used in **paper I** to characterize the surface structure of Cu(100) during oxidation by CO_2 dissociation.

3.2.1 X-ray photoelectron spectroscopy

The idea behind XPS is the photoelectric effect, thus, the surface is irradiated by photons which emits electrons. In XPS, a sample is exposed to x-rays. This exposure creates core-electron holes in the sample atoms, which kinetic energy is measured by an analyzer. The kinetic energy of the ionized photoelectrons is obtained as [82]$^{p.44}$,

$$E_{kin}=h\nu-E_b-\Phi_A \tag{3.8}$$

Here E_{kin} is the kinetic energy of the photoelectron measured at the analyzer, E_b is the core-electron binding energy and Φ_A is the work function of the analyzer, which is constant and can be measured by matching the energy scale to the Fermi edge of a reference sample. The intensity of the XPS spectra is directly proportional to the number of photoelectrons, hence, a quantitative measurement of the atomic species in the sample can be obtained. A schematic representation of X-ray photoelectron spectroscopy is shown in Figure 3.2

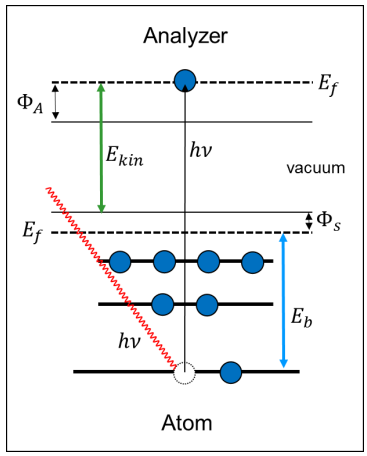

Figure 3.2: XPS schematics. Adapted from Ref.[82]$^{p.44}$

Of special interest is the effect of *chemical shifts*, thus, how the core-electron binding energy depends on the chemical environment. The chemical shift can in a simple picture be explained by the electrostatic potential experienced on an atom because of the chemical bonding changing charge localization [82]$^{p.48}$.

XPS measurements are generally conducted at ultra high vacuum (UHV) conditions, so that the atmosphere around the XPS analyzer does not block the emitted photoelectrons by inelastic scattering. This condition can, however, be circumvented by the use of an ambient pressure cell (usually in the order of $\sim$ 1 mbar), that allows for in-situ operando analysis of catalytic reactions, as it is done in **paper I** and **paper II**. XPS peaks can, regardless of the vacuum conditions, be hard to assign to a specific species on the system. Hence, the experimental characterization can be complemented with theoretical/computational tools, such as CLS calculations.

3.2.2 Core-level shifts

Core-level shift calculations with DFT are known to be in fair agreement with XPS measurements for simple metal systems [83–85]. The nature of the chemical shift can be treated under two different approximations [86]. One being the *initial state approximation*, where the screening of the core-hole by the valence electrons is neglected. The other one being the *final state approximation* that does account for the screening of the core-hole [86]. This approximation is also known as the *complete screening* picture. The final state approximation relies on three assumptions [87]. *i)* The core-hole recombination

is slower than the photoelectron emission process. *ii)* The valence electrons are in the ground state upon core ionization and *iii)* Structural relaxation is neglected upon ground state relaxation of the valence electrons. Experimentally, the binding energy measured is affected by the core-hole screening. Hence, shifts should be treated with some screening.

In the initial state approximation, the CLS can be calculated by use of the Kohn-Sham eigenvalues as [84],

$$E_{CLS} = [\epsilon_C - \epsilon_f] - [\epsilon_C^{ref} - \epsilon_f^{ref}] \tag{3.9}$$

Where ϵ_C and ϵ_f are the KS eigenvalue of the core-state of interest and the Fermi energy [84]. Similarly, ϵ_C^{ref} and ϵ_f^{ref} are the KS eigenvalue of the core-state of interest and the Fermi energy of a reference system. The first square bracket in Equation (3.9), is the core-electron binding energy in the initial state approximation [84]. In the complete screening picture, the CLS can be calculated according to,

$$E_{CLS} = \left[E^* - E^0\right] - \left[E^*_{ref} - E^0_{ref}\right] \tag{3.10}$$

Where E^* and E^*_{ref} are the ground state energy of the core-ionized system of interest and reference system, respectively. E^0 and E^0_{ref}, are the ground state energy of the unperturbed system and reference system, respectively.

There are different approaches on how to calculate the energies of the ionized systems. Specifically, in all-electron calculations, like we do with PAW potentials, one can remove the core-state from the PAW potential, hence generating a PAW potential with a core-hole. This approach leads to a charged system which can be corrected by either adding one electron to the valence or by filling the simulation cell with evenly an distributed jellium. CLS on oxides and semiconductors must be corrected with a jellium, as adding electrons to the valence will introduce non-physical states in the conduction band [87]. Another approach to calculate the energies of the ionized systems it to substitute the atom to be ionized with the neighboring species in the periodic table. This approach is known as the Z+1 approach. In this thesis, we use the PAW potential approach with an electron hole in the O 1s shell [38]. In **paper I**, the CLS are calculated in reference to an oxygen atom in the backside of the Cu(100) slab. This means equation 3.10 is reduced to,

$$E_{CLS} = \left[E^* - E^*_{ref}\right] \tag{3.11}$$

3.3 Analysis of electronic structure

3.3.1 Bader charge analysis

A way to study changes on the surface caused by adsorption of molecular species, like H_2 and H_2O, is with an analysis of charge transfer. This method can elucidate electronic changes at the surface, like charge localization and change in oxidation state on surface atoms or adsorbate characterization. Bader charge analysis is one way to analyze the charge distribution in the system. In this method, the electronic density of a system can be divided into single localized maxima [88]. These maxima are separated from each other by the, so-called, *zero-flux surfaces*, creating volumes in space where the charge is concentrated. The zero-flux surface is described as a 2-D surface on which the charge density is a minimum normal to the surface i.e,

$$\nabla \rho (\mathbf{r}) \cdot \mathbf{n} (\mathbf{r}) = 0 \tag{3.12}$$

Here $\mathbf{n}(\mathbf{r})$ is a unitary normal vector to the surface [89]. This surface defines volumes where the charge localizes. This way of partitioning electronic charge can be exploited to study charge localization and transfer on extended systems. This was done by Henkelman and co-workers [88], who developed a grid-based algorithm for the decomposition of charge following Baders approach. In this algorithm, a path of steepest ascent is followed along the charge density gradient between neighboring points in the grid. By following this approach, the maxima of charge density is found, and the path followed is used to define the Bader volume upon which integration is to be made to determine the total charge in the volume [88, 90, 91]. A schematic representation of charge distribution using the Bader-methods is shown in Figure 3.3.

In this thesis we used the Bader charge analysis in **paper I** and **III** to analyze the charge distribution upon surface oxidation and hydroxylation, respectively.

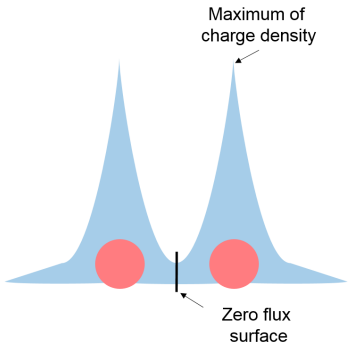

Figure 3.3: Bader charge distribution on an atomic system. Atoms are shown in pink and electron density as faded blue. Adapted from Henkelman's group web-page.

3.3.2 Density of States

Another important electronic structure analysis technique is the Density of States (DOS) analysis. The DOS refers to the number of occupied states per unit of energy (E). DOS analysis facilitates electronic structure understanding, as it shows how the electronic structure is distributed. This makes it possible to observe possible changes in the valence and/or conduction band in the case of an oxide, or the widening (or contraction) of the d-band, in the case of metals. The expression for the DOS is given, as [75]$^{p.96}$,

$$\rho\left(E\right)=\frac{1}{N}\sum_{i,\mathbf{k}}\delta\left(\epsilon_{i,\mathbf{k}}-E\right)=\sum_{i}\int_{\Omega_{BZ}}\delta\left(\epsilon_{i,\mathbf{k}}-E\right)\frac{d\mathbf{k}}{\Omega_{BZ}} \tag{3.13}$$

Where, N is the total number of k-points and $\epsilon_{i,\mathbf{k}}$ refer the energy of the KS-eigenstates ϕ_i. Further information on the origin of the contributions to the DOS can be determined. This can be done by accounting for the contributions from the orbitals (projected DOS) of any species on the system. The orbital contributions (PDOS) are calculated by projecting the momentum states onto a basis set, this is written as [92]$^{p.61}$,

$$PDOS=\rho\left(\psi_{l,m},E\right)=\sum_{i}|\left\langle\psi_{l,m}|\phi_i\right\rangle|^2\delta\left(E-E_i\right) \tag{3.14}$$

Where $\psi_{l,m}$ is the orbital projection in terms of the quantum numbers for angular momenta (l,m). It should be noted that, in practice, we replace the delta function with a Gaussian function. In this thesis, we have made use of DOS and PDOS analysis in **paper III** to explore the change in electronic structure upon surface hydroxylation.

Chapter 4

CO_2 activation on copper and indium oxide

In this chapter we present our results for CO_2 activation as this is the first step in methanol synthesis on copper and indium oxides surfaces. Putative reaction mechanisms are presented and the drawbacks and open questions are discussed.

4.1 CO_2 activation and reduction to CH_3OH

Synthesis of methanol is industrially done on a $Cu/ZnO/Al_2O_3$ catalyst. The overall reaction is,

$$CO_2 + 3H_2 \longleftrightarrow CH_3OH + H_2O \tag{4.1}$$

The enthalpy change for the forward reaction is ΔH = -57.86 kJ/mol (-0.60 eV) [93]. The reaction is performed at high pressures (1-10 MPa) due, in part, to the inertness of CO_2 [i].

In the literature, copper-based surfaces have been used to elucidate the detailed reaction mechanism. Grabow and Mavrikakis explored the possibility of methanol synthesis on Cu(111) from both CO and CO_2 with a combined DFT and mean-field microkinetic modelling (MKM) approach [93]. They found that the CO route proceeds through formyl (HCO), formaldehyde (H_2CO), methoxy (H_3CO) and finally to methanol (H_3COH). Methanol synthesis from CO_2 was in Ref. [93] studied via the Reverse Water-Gas shift (RWGS) reaction. In RWGS, CO_2 reacts with H to carboxyl (COOH) and to CO + H_2O, which then merges with the CO route described. The RWGS mechanism is illustrated in Figure 4.1, in the right lower cycle. Additionally, Grabow and Mavrikakis proposed two other reaction mechanisms for CO_2 hydrogenation. Both mechanisms begin with CO_2 hydrogenation to formate (HCOO), as can be seen in the left cycle in Figure 4.1. The mechanisms split from the formate (HCOO) into two paths. I) One leads to a formic

[i] The dissociative sticking coefficient of CO_2 on Cu(100) is on the order of 10^{-12}[94].

acid intermediate (HCOOH) and then to hydroxymethoxy (H_2COOH). This is followed by splitting of the OH group to make formaldehyde (H_2CO), which hydrogenates to a methoxy (H_3COH) and finally to methanol (H_3COH). II) The second mechanism, proceeds from the formation of formate and leads to the formation of dioxymethylene (H_2CO_2), which hydrogenates to hydroxymethoxy (H_2COOH) and then follows the same route as the first mechanism. It was found that the formic acid route (HCOOH) was preferred as compared to the dioxymethylene one (H_2CO_2) [93]. It was furthermore suggested, from their MKM, that at typical industrial conditions, the CO_2 routes are the main routes (66%) for CO_2 hydrogenation to methanol [93]. Reichenbach *et al.* investigated, with a global optimization of the catalyst structure and DFT calculations for the reaction pathway, the hydrogenation of CO_2 to methanol on a inverse catalyst ZnO/Cu(111) [31]. The purpose of this study was to elucidate the nature of the active site for CO_2 reduction. It was suggested that the reaction occurs at the Cu/ZnO interface and that it proceeds from CO_2 to a formate (HCOO) intermediate, hence avoiding the CO intermediate. The formic acid (HCOOH) and dioxymethylene (H_2CO_2) routes were compared and a slight preference for the dioxymethylene (H_2CO_2) route [31]. They suggest that the formation of formate (HCOO) is critical for a selective hydrogenation of CO_2 to methanol. This is supported by carbon labeling measurements, which suggest that the reaction happens mostly via CO_2 on the copper catalyst [95]. Despite the considerable work, there is no consensus on the dominant reaction mechanism for methanol synthesis over the Cu-catalyst [30–34], or the nature of the site [96, 97].

A drawback with the copper-based catalyst is that it deactivates rapidly due to sintering [23, 24] and that CO_2 adsorption is hindered by surface oxidation [34, 37, 38]. Understanding the process of adsorption and dissociation of CO_2 could provide information on the requirements for CO_2 activation. Moreover, understanding the oxidation process and how this affects the adsorption of CO_2 on the surface on is a necessary step to understand the reasons behind oxygen induced copper deactivation. In this thesis we focus on the early-stage oxidation of Cu(100), to understand the hindering of CO_2 adsorption upon oxidation of the surface. Moreover, a reaction mechanism for CO_2 dissociative adsorption, responsible for the oxidation of Cu(100) is proposed.

In recent years, In_2O_3 has attracted considerable attention in connection to CH_3OH synthesis from CO_2, thanks to measurements showing high activity, selectivity and durability [39–42, 98]. When supported on ZrO_2, this oxide has been reported to exhibit a 100% selectivity with less than 10% loss in activity over a 1000 hours of reaction under typical

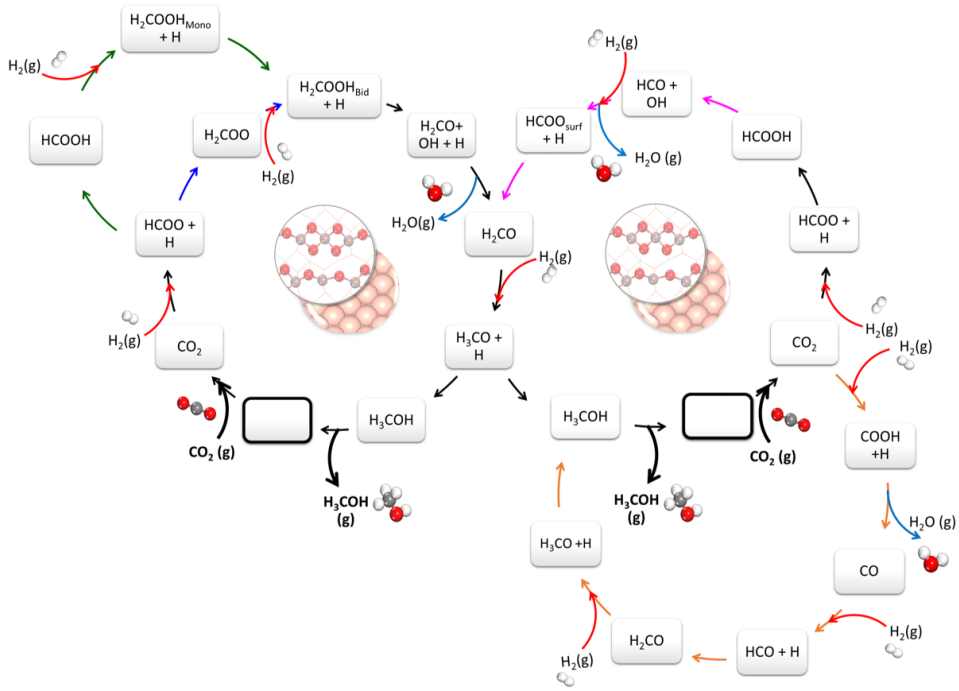

Figure 4.1: Schematic representation of proposed reaction mechanism for CO_2 reduction to CH_3OH.

methanol-synthesis conditions (573 K, 5 MPa, 4:1 ratio H_2/CO_2)[39]. The high selectivity in the temperature range (473-573 K) has been shown experimentally to be linked to a suppression of the RWGS reaction [40]. Moreover, ZrO_2 has been suggested to hinder indium oxide over-reduction [39]. In a recent theoretical work [43], a reaction mechanism that quenches oxygen vacancies has been proposed for the reduction of CO_2 to CH_3OH on $In_2O_3(110)$ [43]. This mechanism is based on hydrogen induced oxygen vacancies. This is followed by a quenching of the vacancy with CO_2. From here, CO_2 follows a HCOO to an HCOOH route. At this stage, unlike on copper surfaces, the loss of the OH-group takes place, and an $HCOO_{surf}$ intermediate is formed. The mechanism follows from this step to H_2CO, a methoxy and finally to H_3COH [43]. However, this mechanism appears to be in conflict with the experimental evidence of the suppression of the RWGS, as CO_2 is known to be unable to quench vacancies [40].

This conflicting result suggests that the reaction at the oxide surface does not follow the suggested path [43, 44]. Moreover, surface hydroxylation effects are neglected on Ref. [43,

44], regardless of the experimental evidence of a high degree of surface hydroxylation[98]. Hence, exploring the thermodynamically preferred surface hydroxylation and the actual role of vacancies in the reaction mechanism is required to understand why In_2O_3 is an effective catalyst for CO_2 hydrogenation to methanol. Both aspects are addressed in this thesis.

A possible reaction mechanism, that does not require oxygen vacancies and that follows all the relevant intermediates suggested in Ref.[43] is presented in Figure 4.1 in purple lines in the right top cycle. Here, CO_2 hydrogenation proceeds through the formation of formate (HCOO), to formic acid (HCOOH) after which the OH group is lost to make formyl (HCO), from this species formate is formed using a surface oxygen $HCOO_{surf}$. The species is then hydrogenated to formaldehyde (H_2CO), methoxy (H_3CO) and finally to methanol (H_3COH).

4.2 Activation of CO_2 on copper

In **paper I** and **II**, we investigated the dissociative adsorption of CO_2 on Cu(100) and the oxidation of the surface as a result of this process. The oxidation of Cu(100) is known to cause a surface reconstruction once a 0.5 monolayer (ML) has been reached [34, 99–105]. Moreover, the oxidation of the surface is known to hinder the adsorption of CO_2 [34]. Our work was performed in a collaboration between experiment and theory. Experimentally, AP-XPS measurements were performed. Whereas on the theory side, *ab initio* thermodynamic calculations were performed to provide surface stabilities and core-level shifts (CLS) were calculated to obtain spectroscopic signatures. The experimental continuous tracking of the change of the O 1s core-electron binding energy as a function of exposure together with the calculations allow for a deeper understanding on the nature of the dissociation process as well as an understanding on the early-stage oxidation of Cu(100).

The surface science approach to understand the activation and reaction of CO_2 to methanol has been applied since the 90's [106, 107]. In more recent years, it was shown experimentally that the most exposed facets for methanol synthesis on a copper nanoparticle supported on ZnO are the (111) and (100) facets [108]. Cu(111) is the most stable surface with a surface energy of $\gamma_{(111)} = 1.29$ J/m^2. However, CO_2 does not adsorb on this surface. Cu(100), has a surface energy to be $\gamma_{(100)} = 1.43$ J/m^2 and is able to adsorb CO_2. Hence, we decided to study this surface structure to attain understanding of basic principles for CO_2 dissociative adsorption and surface oxidation.

4.2.1 Initial oxidation of Cu(100) by CO_2 dissociation

In **paper I**, we studied the early-stage oxidation of Cu(100). Experimentally, this was done by exposing the Cu(100) to CO_2 at a pressure of 0.4 mbar at a temperature of 373.15 K and tracking, by AP-XPS, the O 1s binding energy during exposure. A gradual shift of the binding energy was found with increasing oxygen coverage. A peak at 529.5 eV assigned to atomic oxygen at the surface, was found to shift to a higher energy (530 eV) at high oxygen coverage. This result is in agreement with previous experimental reports [34, 109]. Computationally we found that oxidation of Cu(100) occurs via the initial formation of an ordered p(2×2) overlayer at 0.25 ML followed by the reconstructed $(2\sqrt{2} \times \sqrt{2})$R45° (MR) structure at 0.50 ML. The surface stability analysis, along with the surface structures explored, are shown in Figure 4.2.

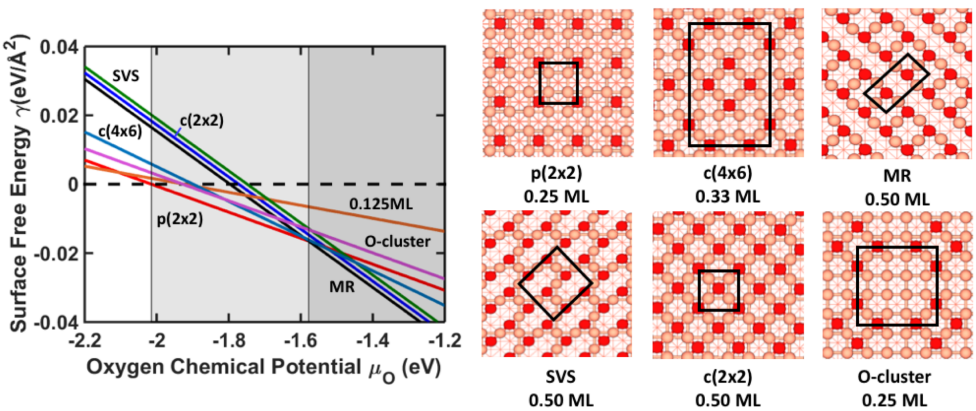

Figure 4.2: Surface stability of Cu(100) as a function of oxygen chemical potential (μ_O) at a temperature of 373 K.

Core level shifts for O 1s are calculated within the complete screening approximation for the different surface structures. Our results are compared to the experimental AP-XPS data. We find a shift of the O 1s biding energy of 0.7 eV between the p(2×2) and the MR structure. This result is in reasonable agreement to the experimental measure to higher binding energy of 0.5 eV between the low and high oxygen covered structures. This suggests that the energy peak at 529.5 eV and 530 eV, can be assigned to the p(2×2) and MR structures, respectively. The calculated CLS, with respect to a 0.125 ML oxygen structure, along with the experimental AP-XPS spectra are shown in Figure 4.3.

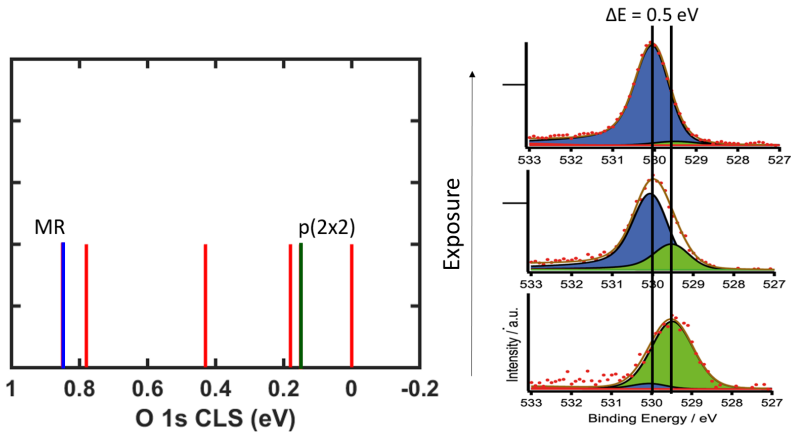

Figure 4.3: Core-level shift of the O 1s for the studied surface structures. The left panel shows the CLS calculated with respect to their corresponding reference system, 0.125ML in a $(2\sqrt{2} \times 2\sqrt{2})$R45° unit cell. The reference system for c(4×6) is the corresponding c(4×6) at 0.04 ML. Right: AP-XPS spectra of O 1s binding energy as a function of exposure to CO_2

We found the CLS to correlate to the charge of the copper atoms bound to the surface oxygen. We rationalized this as a direct electrostatic interaction between the reduced copper and the core electrons in oxygen. As copper changes oxidation state, the O 1s state is stabilized thanks to the electrostatic interaction. This can be understood as an initial state effect. Writing the core-electron binding energy shift of state i, relative to the binding energy of a reference system, as [110],

$$\Delta E_i = kq_i + \sum_{j \neq i} \frac{q_j}{R_{ij}} \tag{4.2}$$

Where, k is the Coulomb repulsion integral between core and valence electrons, q_i is the charge on atom i and R_{ij} is the interatomic distance between the i and j nuclei. It becomes clear that the positive charge on the O-bound copper atoms affects the core-electron biding energy of the O 1s state.

4.2.2 Dissociative adsorption of CO_2 on Cu(100)

In **paper II**, we studied the dissociative adsorption mechanism of CO_2 on Cu(100). We found that the dissociation of CO_2 on Cu(100) takes place predominantly at single atomic steps. The experimental findings can be compactly presented as an oxygen uptake curve, where the low (529.5 eV) and high binding (530 eV) energy peaks associated to the p(2×2)

and MR structures are tracked as a function of exposure to CO_2, See Figure 4.4. An important aspect is the linearity of the uptake curve in the region between 0.25 and 0.45 ML, which suggest that the active site number remains unaltered. After 0.45 ML, an exponential decay sets in, indicating that the active sites are being consumed.

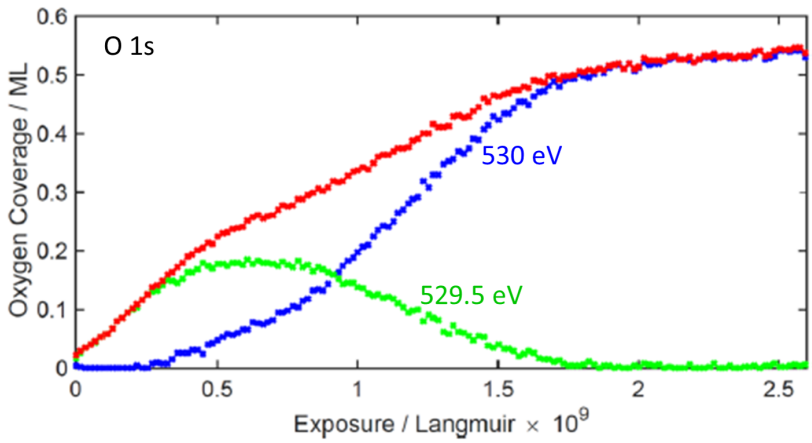

Figure 4.4: O 1s binding energy evolution of adsorbed oxygen as a function of exposure to CO_2.

To study the dissociative adsorption of CO_2 we propose a simple reaction mechanism where CO_2 oxidizes the surface and CO desorbs. This mechanism is composed of two intermediates, CO_2^* (bound) and CO^*+O^* (bound). CO_2 adsorption (TS_1) and CO_2 dissociation (TS_2) are activated. On the pristine Cu(100) surface, these barriers are 0.55 and 0.83 eV, respectively. The calculated energy landscape for this process on the pristine Cu(100) is shown in Figure 4.5. CO_2 adsorbs on the metal surface in a $CO_2^{\delta-}$ configuration over a hollow site. We find that the adsorption of CO_2 on an O-covered surface is strongly dependent on the relative position of the adsorbed oxygen with respect to the adsorption site. However, if CO_2 adsorption is possible, the destabilizing effect on the adsorbates and subsequent energy barriers is small ($\sim$ 0.1 eV). This explains the change in slope in Figure 4.4 at 0.25 ML. The linearity of the oxygen uptake curve is explained by a conservation of the active sites during the reaction up to a coverage of 0.45 ML. We speculated that the active sites could be monoatomic steps. The possible effect of steps was evaluated by considering a stepped Cu(611). This surface can be described as two asymmetrically sized (100) terraces joint together by a (111) step. The linear slope in Figure 4.4 is explained by the dissociation taking place on an step site and subsequent

oxygen diffusion to the terrace. The barrier for dissociation (TS_2) is significantly lower on the step than on the open surface (TS_2 = 0.57 eV), while the first barrier is only slightly higher (TS_1 = 0.60 eV). Additionally, oxygen diffusion to the terrace explains why the number of active sites remains unchanged. The potential energy diagram comparing Cu(100) and Cu(611) can be seen in Figure 4.5.

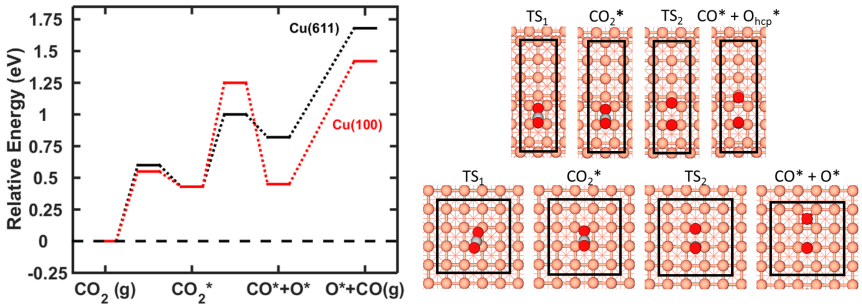

Figure 4.5: CO_2 dissociation mechanism on Cu(100) and Cu(611). Left: Potential energy diagram. Right: Surface structures of intermediate states (Top Cu(611) and bottom Cu(100)).

The work suggest a path for oxidation of Cu(100) where CO_2 adsorbs dissociatively predominantly at the step site. Oxygen diffusion to the (100) terrace leads to the formation of an ordered p(2×2) overlayer at 0.25 ML, associated to an O1s binding energy of 529.5 eV. The continuous dissociation of CO_2 eventually makes the surface to reconstruct into the $(2\sqrt{2} \times \sqrt{2})$R45° (MR) structure at 0.50 ML, which is observed in the spectroscopic signature of the O 1s state by shifting to a higher biding energy of 530 eV. Given the closed-shell nature of CO_2, van der Waals effects are expected to stabilize its interaction with the metallic Cu(100). The effect of van der Waals interactions was evaluated with the use of the Chalmers-Rutgers vdW-DF-cx functional [66]. We find that van der Waals interactions stabilizes the adsorption of CO_2 on the surface, however, it also stabilizes all other steps in the reaction mechanism to a similar degree. Thus, the net effect on the calculated barriers for adsorption and dissociation is small.

A mean-field microkinetic model was developed to test the validity of the reaction mechanism and energy landscape obtained for CO_2 dissociative adsorption. The dissociative adsorption is modeled as a set of two elementary reactions were the surface is ultimately oxidized by CO_2,

$$CO_2(g) + ^* \longleftrightarrow CO_2^* \tag{4.3}$$

$$CO_2^* \rightarrow O^* + CO(g) \tag{4.4}$$

The neglecting of CO re-adsorption is motivated by the experimental continuous pumping, and we assume that CO leaves the surface once formed. The experimental values for CO_2 pressure (P_{CO_2}= 3x10^4 Pa) and temperature (T= 375 K) were utilized. A re-scaling of the maximum oxygen coverage is considered to account for saturation previous to surface reconstruction, at an oxygen coverage of 0.5 monolayer. The activation energies calculated were utilized to determine the rate coefficients. The time evolution of the oxygen coverages over Cu(100) and Cu(611) are shown in Figure 4.6.

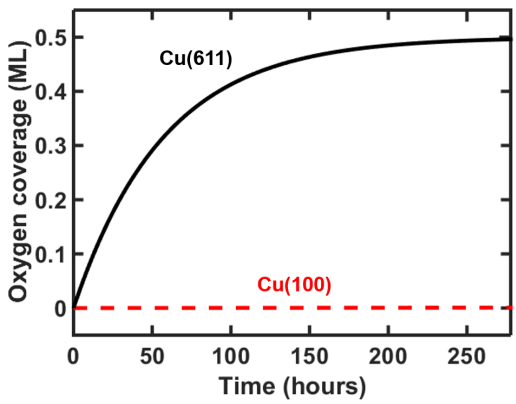

Figure 4.6: Oxygen coverage as a function of time from CO_2 dissociative-adsorption mean-field microkinetic model on Cu(100) and Cu(611). Dashed and solid lines show results for Cu(100) and Cu(611), respectively.

From the experimental observations we know that oxidation of the surface occurs in a matter of hours. Using the DFT values, Cu(611) saturates at a coverage of 0.5 ML at approximately $\sim$ 250 hours. This means our results are 2 orders of magnitude off with respect to experimental observations. This discrepancy between theory and experiment translates to an overestimation of the dissociative barrier of roughly 0.2 eV on Cu(611) with respect to experiment. Reducing the dissociation barrier on Cu(100) by 0.2 eV in our MKM still takes over 1600 hours to reach 0.5 ML. Hence, it is clear that oxidation of the surface is strongly determined by the dissociation at steps.

4.3 Activation of CO_2 on indium oxide

In_2O_3 supported on ZrO_2 has been reported to be highly active for the reduction of CO_2 to H_3COH in Ref. [39]. The catalyst was characterized by XRD and found to expose $In_2O_3(222)$ facets after reaction. In_2O_3 exists in three polymorphs, two bixbyite (with space groups 199 and 206) and a corundum (space group 167). We optimized the three bulk structures and simulated the corresponding XRD patter for comparison with the experimental data. We found that the bixbyite structure with space group 206 is the one reported in Ref. [39].

The stable In_2O_3 surface is $In_2O_3(111)$, with a surface energy of $\gamma_{(111)} = 0.78$ J/m^2. However, we found this surface to be chemically inert for CO_2 adsorption. The less stable $In_2O_3(110)$, with a surface energy of $\gamma_{(110)} = 1.05$ J/m^2, is, however, active for CO_2 adsorption. Moreover, $In_2O_3(110)$ has been reported in the literature as a model system for CO_2 reduction to H_3COH [43, 44]. Hence, we decided to follow the literature and consider $In_2O_3(110)$ as a model system to attain a basic mechanistic understanding for CO_2 activation on In_2O_3.

4.3.1 Determination of $In_2O_3(110)$ active phase

In **paper III**, we investigated the effect of surface hydroxylation of In_2O_3 by H_2 and H_2O dissociation. By making use of *ab initio* thermodynamics we can elucidate the stable surface structure at typical methanol synthesis conditions (573 K, 5 MPa, 4:1 ratio H_2/CO_2 and 1 MP). We find that, in both cases, the surface will heavily hydroxylate. These results are in accordance to experimental evidence of surface hydroxylation upon hydrogen exposure at (473 to 573 K)[98]. Our results are shown in Figure 4.7. Here, we defined a full coverage of the surface (100%) when there is as much hydrogen on the surface as are oxygen sites. Hydroxylation with H_2 was studied at five hydrogen coverages (16, 50, 66, 83 and 100%). For the thermodynamic stability analysis, we limited our search to homolytically dissociated H_2. Similarly, hydroxylation with H_2O was studied at six hydrogen coverages (16, 33, 50, 66, 83 and 100%). In this case, we considered H adsorption on an oxygen site and OH-group adsorption on an In-site. Both methods of hydroxylation lead to an 83 % hydrogen coverage on the surface. The stable surface structure under both hydroxylation conditions can be seen in Figure 4.8.
The effect of hydroxylation is different for H_2 and H_2O. A Bader charge analysis of the surface upon hydroxylation with H_2 reveal that the undercoordinated In-site at the surface change oxidation state, from In^{3+} to In^{2+}. However, the same kind of analysis

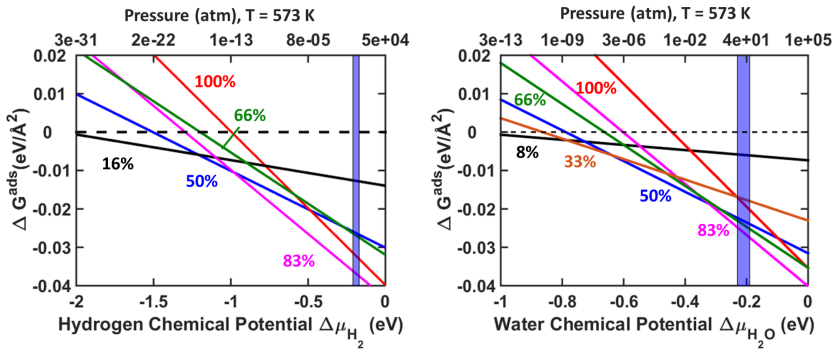

Figure 4.7: Surface stability of $In_2O_3(110)$ as a function of hydrogen (left) and water (right) chemical potential (μ_{H_2}, μ_{H_2O}) or pressure at a temperature of 573 K. The results are given with respect to the pristine surface at zero energy. Experimental conditions, 1-5 MPa (10-50 bar), are indicated by a purple fringe.

upon hydroxylation with H_2O shows little change on the oxidation state of the In-sites, with the charge being localized on the OH groups. Additionally, surface relaxation upon hydroxylation is much less severe with H_2O than with H_2, which is related to the In-sites retaining their In^{3+} ionic site in the case of H_2O adsorption. We find also that the creation of oxygen vacancies is thermodynamically driven for a limited number of oxygen-sites only at high hydrogen coverage. At low coverage, homolytically dissociative adsorption of H_2 is the preferred case, for all oxygen-sites.

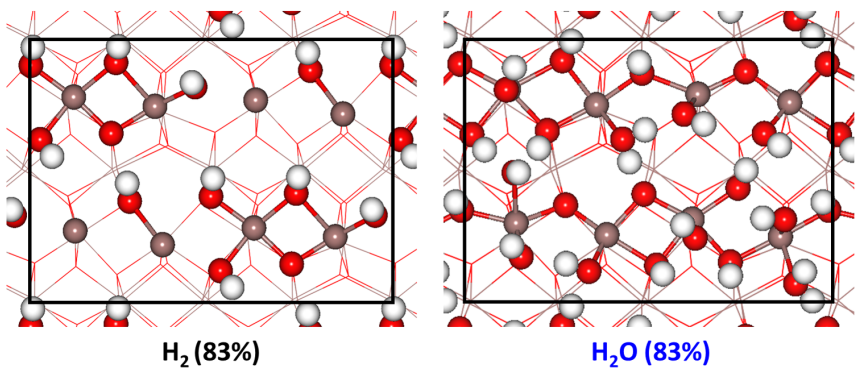

Figure 4.8: Thermodynamically stable surface structures upon hydroxilation by dissociated H_2 (left) and H_2O (right), at methanol synthesis conditions (537 K, 1-5 MPa).

Our results shows significant change in electronic structure upon homolytic hydroxylation with H_2. This is corroborated with a density of state analysis, where the total DOS and projected DOS (PDOS) are analyzed for the pristine and hydroxylated surface. A significant widening of the valence band, due to the O 2s/O 2p and H 1s interaction (overlap), at the bottom of the valence band and above the Fermi energy, is observed upon hydroxylation (See Figure 4.9).

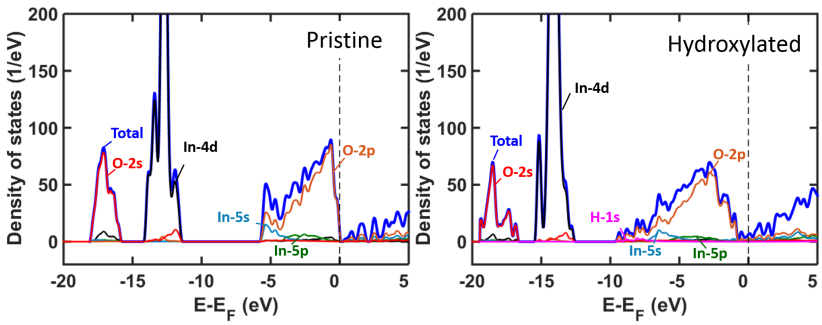

Figure 4.9: Density of States analysis on pristine (Left) and fully hydroxylated (right) $In_2O_3(110)$.

Our results suggest that, at methanol-synthesis conditions, $In_2O_3(110)$ will probably have some vacancies and will be heavily hydroxylated. Moreover, we find that theoretical description of the reduction of CO_2 on $In_2O_2(110)$ should take into account hydroxylation of the surface. Given the redox capacity of the undercoordinated indium sites on the surface, a description without sufficient hydroxylation is likely to alter the chemical properties of the surface.

4.3.2 Adsorption of CO_2 on $In_2O_3(110)$

In **paper III**, we also investigated the activation and adsorption of CO_2 on pristine and H/covered, defective and defect-free $In_2O_3(110)$. This was done in order to determine the role of oxygen vacancies on the mechanism for methanol synthesis. We found that adsorption in oxygen vacancies is thermodynamically unfavorable, regardless of the hydrogen coverage at the surface. This result is in agreement with the observed suppression of the RWGS reported by Bielz *et al.*[40]. However, adsorption of CO_2 in a $CO_2^{\delta-}$ configuration is energetically feasible, regardless of the hydrogen coverage on the surface. On the purely pristine surface, CO_2 appears to adsorb preferably on a carbonate-like configuration,

suggesting that this species might be found on In_2O_3 with low H-coverage.

We calculated the activation barrier for CO_2 adsorption on the stable hydroxylated $In_2O_3(110)$, at methanol synthesis conditions, in three situations. I) CO_2 adsorption in a vacancy. II) CO_2 adsorption near a vacancy and III) CO_2 adsorption on a fully hydroxylated surface without vacancies. We find the activation energies to be, 1.67, 0.82 and 0.48 eV, respectively. Moreover, the backwards barriers for the three cases are found to be, 0.61, 0.02 and 0.37 eV. The results suggest that the CO_2 adsorption is more likely to occur in a fully hydroxylated surface, without vacancies. Thus, a reaction mechanism that requires quenching of oxygen vacancies by CO_2 adsorption, is unlikely to be responsible for the reduction of carbon dioxide to methanol on In_2O_3. Instead, adsorption in a CO_2^- configuration, facilitated by the reduced indium sites, is energetically preferred. The full reaction pathway and the configurations described are shown in Figure 4.10.

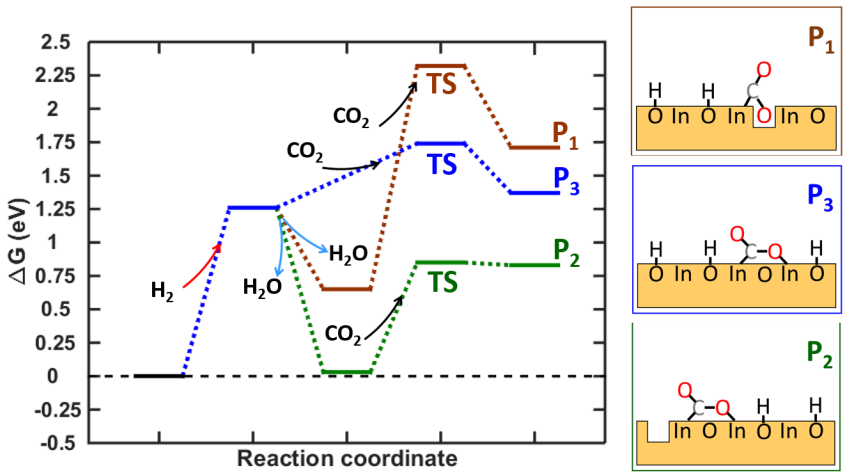

Figure 4.10: Gibbs free energy diagram of reaction mechanisms for CO_2 adsorption on $In_2O_3(110)$ at experimentally relevant reaction conditions (573 K, 5MPa (H_2/CO_2 = 4:1).

Our results suggest that oxygen vacancies, although present at reaction conditions, do not play a significant role on the adsorption of CO_2. Instead we suggest that it is the redox capacity of the indium sites that is likely to facilitate the adsorption of CO_2 on this oxide.

Chapter 5

Conclusions and Outlook

This thesis has been aimed to rationalize the activation and adsorption of CO_2 on copper and indium oxide surfaces, under thermodynamically relevant conditions for methanol synthesis. The understanding of this reaction step, and of the active phase of the catalyst, are particularly important for the rational design of catalysts for reduction of CO_2 to methanol.

The oxidation process of Cu(100) and the dissociative-adsorption mechanism of CO_2 were studied in a coupled theory/experiment approach. This was done by making use of DFT calculations, coupled with *ab initio* thermodynamics, and core-level spectroscopy (AP-XPS). Some general understanding is drawn from our investigation. We found that copper oxidizes from a pristine surface, to a p(2×2) overlayer at 0.25 ML followed by the reconstructed $(2\sqrt{2} \times \sqrt{2})$R45° (MR) structure at 0.50 ML. Moreover, the dissociative adsorption of CO_2 on Cu(100) occurs most predominantly at the step of the surface, and oxygen diffusion and recombination with CO on the step keeps the site free for the reaction to continue.
Additionally, we studied the effect of surface hydroxylation, with H_2 and H_2O, on In_2O_3(110) and the role of oxygen vacancies for CO_2 adsorption. This was done exclusively with the use of DFT calculations. We conclude that at methanol synthesis conditions, the surface will heavily hydroxylate, both with H_2 and H_2O. However, the chemical nature of the surface is strongly dependent on the molecules that adsorb.
Hydroxylation with H_2 leads to a change in oxidation state of undercoordinated indium sites, from In^{3+} to In^{2+}, which is not observed with H_2O. Furthermore, our results indicate that oxygen vacancies are thermodynamically relevant only at high hydrogen coverage. Nevertheless, oxygen vacancies do not facilitate the adsorption of CO_2. Instead, we suggest that the redox capacity of the undercoordinated In-sites is responsible for the adsorption of CO_2. Our results are in qualitative agreement with the experimental observation of heavy hydroxylation and the suppression of the reverse water gas shift on indium oxide.

By making use of coupled DFT calculations with *ab initio* thermodynamics and ambient

pressure X-ray photoelectron spectroscopy (AP-XPS) we have tried to bridge the so-called pressure gap. Despite of this, our results suffer, to some extent, still from the materials and pressure gaps, given that we work with model systems that are far from the real catalysts at reaction conditions. Additionally, we have chosen to make our DFT calculations with GGA functionals. This is know to be reasonable for metallic systems, but it is a crude approximation for oxides. A comparison should be done with approximations that are known to better describe oxides, such as DFT+U approach or hybrid functionals.
Regardless of the shortcomings of the model systems and methods we use, systematic work on simplified models must be done to gain general understanding of catalytic reactions, like critical elementary steps and active sites. Once this knowledge is obtained, we can increase the complexity of the considered systems.

The ultimate goal of this project is to understand the electronic structure basis for the high activity and selectivity of In_2O_3/ZrO_2 for CO_2 hydrogenation to CH_3OH. Hence, several open questions remain to be answered. The work to be done relates to the proposal of a putative reaction mechanism on $In_2O_3(110)$. Moreover, the effect of ZrO_2 is to be investigated as well. Here, it could be useful to study the kinetics of the mechanisms at the surface, as this could validate the probability of a putative reaction mechanism for the hydrogenation of CO_2 to methanol. In addition, it could be interesting to study the diffusion and stability of oxygen below the surface on the copper systems, as the existence of such species has been proposed recently as necessary for the chemical adsorption of CO_2 on O or OH covered copper surfaces.

Finally, it must be noted that the present work highlights the significance of theoretical and computational studies on model systems. Such studies allow the unravelling of underlying mechanisms of chemical reactions, such as CO_2 hydrogenation to methanol, in the hope of aiding in the rational design of more efficient and affordable catalysts.

Acknowledgments

The research presented herein was carried out at the Division of Chemical Physics and Competence Centre for Catalysis at Chalmers University of Technology, Göteborg, Sweden in the period October 2016 to March 2019.

The research was funded by the Knut and Alice Wallenberg Foundation through the project "Atomistic design of catalysts" (No: KAW 2015.0058). Computational time has been granted by SNIC at C3SE (Göteborg), PDC (Stockholm) and Uppmax (Uppsala).

The Competence Centre for Catalysis is financially supported by Chalmers University of Technology, the Swedish Energy Agency and the member companies: AB Volvo, ECAPS AB, Johnson Matthey AB, Preem AB, Scania CV AB, Umicore Denmark ApS and Volvo Car Corporation AB.

Additionally I would like to acknowledge the following people,

My main supervisor, Henrik Grönbeck, for your ever-growing guidance and support and for the always enjoyable discussions throughout this project. Thank you for always having an open door and for helping me understand my results. Let's continue showing them how we roll.

My co-supervisor, Anders Hellman, for your willingness and cheerfulness to discuss both formal and informal topics.

My main experimental collaborators, Benjamin Hagman and Johan Gustafson. For the very fruitful collaboration and for the interesting discussions on our projects together.

My current and past colleagues of the Chemical physics group, for always being willing to give a helping hand and for the friendly atmosphere we all make together. In particular I would like to thank, Lucy, Adam, Noemi, Lin, Unni, Mikkel, Mikael, Michael, Matthias, Baochang, Fredrik, Chris (Dr. Heard), Anna and Maxime.

I would also like to acknowledge the members of the Competence Centre for Catalysis (KCK) and other co-workers at Chalmers for the nice environment for discussion (Both in

and outside of Chalmers). In particular I would like to thank, Andreas, Ting, Johanna, Simone, Carl-Robert, Felix, Peter, Silver, Viktor and Christopher.

I would very much like to acknowledge my girlfriend, İrem, for your infinite patience, understanding and support. My days are always better when I'm with you.

Finally, I want to thank my family. My parents, Alvaro and Dora, for your unconditional love and support. Everything I am is because of you. My siblings, Oliver and Atenas, because you have and always will be my second parents.

We are the lucky ones.
Thank you all!

References

[1] C. T. Campbell. Catalyst-support interactions: Electronic perturbations. *Nature chemistry* **4** (2012), 597–598. DOI: 10.1038/nchem.1412.

[2] S. Zimov, E. Schuur, and F. Chapin. Permafrost and the global carbon budget. *Science* **312** (2006), 1612–1613. DOI: 10.1126/science.1128908.

[3] B. Santer et al. Contributions of anthropogenic and natural forcing to recent tropopause height changes. *Science* **301** (2003), 479–483. DOI: 10.1126/science.1084123.

[4] G. Meehl and C. Tebaldi. More intense, more frequent, and longer lasting heat waves in the 21st century. *Science* **305** (2004), 994–997. DOI: {10.1126/science.1098704}.

[5] P. Ciais et al. Europe-wide reduction in primary productivity caused by the heat and drought in 2003. *Nature* **437** (2005), 529–533. DOI: {10.1038/nature03972}.

[6] J. Hansen et al. Global temperature change. *PNAS* **103** (2006), 14288–14293. DOI: 10.1073/pnas.0606291103.

[7] Intergovernmental Panel on Climate Change. *Climate Change 2014: Mitigation of Climate Change: Working Group III Contribution to the IPCC Fifth Assessment Report*. Cambridge University Press, 2015. DOI: 10.1017/CBO9781107415416.

[8] B. Bajzelj, J. M. Allwood, and J. M. Cullen. Designing climate change mitigation plans that add up. *Env. Sci. Tech.* **47** (2013), 8062–8069. DOI: 10.1021/es400399h.

[9] Energimyndigheten [Swedish Energy Agency]. *Energy in Sweden 2018: An overview*. https://energimyndigheten.a-w2m.se/Home.mvc?ResourceId=5774. Accessed: 2019-03-16.

[10] G. Olah. Beyond oil and gas: the methanol economy. *Angew. Chem. Int. Ed.* **44** (2005), 2636–2639. DOI: 10.1002/anie.200462121.

[11] G. A. Olah, A. Goeppert, and G. K. S. Prakash. Chemical recycling off carbon dioxide to methanol and dimethyl ether: from greenhouse gas to renewable, environmentally carbon neutral fuels and synthetic hydrocarbons. *J. Org. Chem.* **74** (2009), 487–498. DOI: 10.1021/jo801260f.

[12] G. A. Olah, G. K. S. Prakash, and A. Goeppert. Anthropogenic chemical carbon cycle for a sustainable future. *J. Am. Chem. Soc.* **133** (2011), 12881–12898. DOI: 10.1021/ja202642y.

[13] A. Goeppert et al. Recycling of carbon dioxide to methanol and derived products - closing the loop. *Chem. Soc. Rev.* **43** (2014), 7995–8048. DOI: 10.1039/c4cs00122b.

[14] M. D. Porosoff, B. Yan, and J. G. Chen. Catalytic reduction of CO_2 by H_2 for synthesis of CO, methanol and hydrocarbons: challenges and opportunities. *Energy Environ. Sci.* **9** (2016), 62–73. DOI: 10.1039/c5ee02657a.

[15] A. Alvarez et al. Challenges in the greener production of formates/formic acid, methanol, and DME by heterogeneously catalyzed CO_2 hydrogenation processes. *Chem. Rev.* **117** (2017), 9804–9838. DOI: 10.1021/acs.chemrev.6b00816.

[16] S. Kattel, P. Liu, and J. G. Chen. Tuning selectivity of CO_2 hydrogenation reactions at the metal/oxide interface. *J. Am. Chem. Soc.* **139** (2017), 9739–9754. DOI: 10.1021/jacs.7b05362.

[17] R. M. Navarro, M. A. Pena, and J. L. G. Fierro. Hydrogen production reactions from carbon feedstocks: fossils fuels and biomass. *Chem. Rev.* **107** (2007), 3952–3991. DOI: 10.1021/cr0501994.

[18] A. I. Olivos-Suarez et al. Strategies for the direct catalytic valorization of methane using heterogeneous catalysis: challenges and opportunities. *ACS Catal.* **6** (2016), 2965–2981. DOI: 10.1021/acscatal.6b00428.

[19] P. Edwards et al. Hydrogen and fuel cells: Towards a sustainable energy future. *Energy Policy* **36** (2008), 4356–4362. DOI: 10.1016/j.enpol.2008.09.036.

[20] *Alternative Fuels Data Center - Fuel Properties Comparison*. https://www.afdc.energy.gov/fuels/fuel_comparison_chart.pdf. Accessed: 2018-10-29.

[21] D. S. Marlin, E. Sarron, and O. Sigurbjornsson. Process Advantages of direct CO_2 to methanol synthesis. *Front. Chem.* **6** (2018), 4461–4468. DOI: 10.3389/fchem.2018.00446.

[22] K. Cheng et al. "Advances in catalysis for syngas conversion to hydrocarbons". *Advances in catalysis, Vol. 60*. Ed. by Song, C. Vol. 60. Advances in catalysis. 2017, 125–208. DOI: 10.1016/bs.acat.2017.09.003.

[23] J. Sun, I. Metcalfe, and M. Sahibzada. Deactivation of $Cu/ZnO/Al_2O_3$ methanol synthesis catalyst by sintering. *Ind. Eng. Chem. Res.* **38** (1999), 3868–3872. DOI: 10.1021/ie990078s.

[24] M. Twigg and M. Spencer. Deactivation of copper metal catalysts for methanol decomposition, methanol steam reforming and methanol synthesis. *Top. Catal.* **22** (2003), 191–203. DOI: 10.1023/A:1023567718303.

[25] M. Beller, A. Renken, and R. A. van Santen. *Catalysis: From principles to applications*. Weinheim, Germany: Wiley-VCH, 2012.

[26] I. Chorkendorff and W.Niemantsverdriet. *Concepts of Modern Catalysis and Kinetics*. Weinheim, Germany: Wiley-VCH, 2003.

[27] P. Mars and D. van Krevelen. Oxidations carried out by means of vanadium oxide catalysts. *Chemical Engineering Science* **3** (1954). The Proceedings of the Conference on Oxidation Processes, 41–59. DOI: 10.1016/S0009-2509(54)80005-4.

[28] C. Doornkamp and V. Ponec. The universal character of the Mars and Van Krevelen mechanism. *Journal of Molecular Catalysis A: Chemical* **162** (2000), 19–32. DOI: 10.1016/S1381-1169(00)00319-8.

[29] G. Somorjai. The surface science of heterogeneous catalysis. *Surf. Sci.* **299-300** (1994), 849–866. DOI: 10.1016/0039-6028(94)90702-1.

[30] M. Behrens et al. The active site of methanol synthesis over $Cu/ZnO/Al_2O_3$ industrial catalysts. *Science* **336** (2012), 893–897. DOI: 10.1126/science.1219831.

[31] T. Reichenbach et al. Ab initio study of CO_2 hydrogenation mechanisms on inverse ZnO/Cu catalysts. *J. Catal.* **360** (2018), 168–174. DOI: 10.1016/j.jcat.2018.01.035.

[32] M. Hus, D. Kopac, and B. Likozar. Catalytic hydrogenation of carbon dioxide to methanol: synergistic effect of bifunctional Cu/perovskite catalysts. *ACS Catal.* **9** (2019), 105–116. DOI: 10.1021/acscatal.8b03810.

[33] F. Studt et al. The mechanism of CO and CO_2 hydrogenation to methanol over Cu-based catalysts. *ChemCatChem* **7** (2015), 1105–1111. DOI: 10.1002/cctc.201500123.

[34] B. Eren et al. Dissociative carbon dioxide adsorption and morphological changes on Cu(100) and Cu(111) at ambient pressures. *J. Am. Chem. Soc.* **138** (2016), 8207–8211. DOI: 10.1021/jacs.6b04039.

[35] B. Hagman et al. Steps control the dissociation of CO_2 on Cu(100). *J. Am. Chem. Soc.* **140** (2018), 12974–12979. DOI: 10.1021/jacs.8b07906.

[36] M. Behrens et al. The active site of methanol synthesis over $Cu/ZnO/Al_2O_3$ industrial catalysts. *Science* **336** (2012), 893–897. DOI: 10.1126/science.1219831.

[37] B. Eren et al. Structure of the Clean and Oxygen-Covered Cu(100) Surface at Room Temperature in the Presence of Methanol Vapor in the 10-200 mTorr Pressure Range. *J. Phys. Chem. B* **122** (2018), 548–554. DOI: 10.1021/acs.jpcb.7b04681.

[38] A. Posada-Borbón et al. Initial oxidation of Cu(100) studied by X-ray photoelectron spectroscopy and density functional theory calculations. *Surf. Sci.* **675** (2018), 64–69. DOI: 10.1016/j.susc.2018.04.015.

[39] O. Martin et al. Indium oxide as a superior catalyst for methanol synthesis by CO_2 hydrogenation. *Angew. Chem. Int. Ed.* **55** (2016), 6261–6265. DOI: 10.1002/anie.201600943.

[40] T. Bielz et al. Water-gas shift and formaldehyde reforming activity determined by defect chemistry of polycrystalline In_2O_3. *J. Phys. Chem. C* **115** (2011), 6622–6628. DOI: 10.1021/jp111739m.

[41] H. Lorenz et al. Novel methanol steam reforming activity and selectivity of pure In_2O_3. *Appl. Catal., A* **347** (2008), 34–42. DOI: 10.1016/j.apcata.2008.05.028.

[42] T. Umegaki et al. Hydrogen production via steam reforming of ethyl alcohol over nano-structured indium oxide catalysts. *J. Power Sources* **179** (2008), 566–570. DOI: 10.1016/j.jpowsour.2008.01.010.

[43] J. Ye et al. Active oxygen vacancy site for methanol synthesis from CO_2 hydrogenation on In_2O_3(110): a DFT study. *ACS Catal.* **3** (2013), 1296–1306. DOI: 10.1021/cs400132a.

[44] J. Ye, C. Liu, and Q. Ge. DFT study of CO_2 adsorption and hydrogenation on the In_2O_3 surface. *J. Phys. Chem. C* **116** (2012), 7817–7825. DOI: 10.1021/jp3004773.

[45] A. Szabo and N. S. Ostlund. *Modern Quantum Chemistry: Introduction to Advanced electronic structure theory*. Mineola, New York: Dover Publications, 1996.

[46] D. J. Wales. *Energy landscapes: With applications to clusters, biomolecules and glasses*. Cambridge, United Kingdom: Cambridge University press, 2003.

[47] J. Thijssen. *Computational physics*. Cambridge, United Kingdom: Cambridge University press, 2007.

[48] D. R. Hartree. The wave mechanics of an atom with a non-Coulomb central field. Part I. Theory and methods. *Mathematical Proceedings of the Cambridge Philosophical Society* **24** (1928), 89–110. DOI: 10.1017/S0305004100011919.

[49] V. Fock. Näherungsmethode zur lösung des quantenmechanischen mehrkörperproblems. *Zeitschrift für physik* **61** (1930), 126–148. DOI: 10.1007/BF01340294.

[50] P. Hohenberg and W. Kohn. Inhomogeneous electron gas. *Phys. Rev.* **136** (1964), B864–B871. DOI: 10.1103/PhysRev.136.B864.

[51] W. Kohn and L. J. Sham. Self-consistent equations including exchange and correlation effects. *Phys. Rev.* **140** (1965), A1133–A1138. DOI: 10.1103/PhysRev.140.A1133.

[52] I. N. Levin. *Quantum chemistry*. Boston, Massachusetts: Pearson, 2014.

[53] L. H. Thomas. The calculation of atomic fields. *Mathematical Proceedings of the Cambridge Philosophical Society* **23** (1927), 542–548. DOI: 10.1017/S0305004100011683.

[54] E. Fermi. Un metodo statistico per la deteminazione di alcune priorta dell atomo. *Rend. Accad. Naz. Lincei* **6** (1927), 602–607.

[55] R. G. Parr and R. G. Y. Weitao. *Density-Functional Theory of Atoms and Molecules*. Accessed: 2019-03-03; https://ebookcentral.proquest.com/lib/chalmers/detail.action?docID=271295. Oxford University Press, 1987.

[56] J. Janak. Proof that $\frac{\partial E}{\partial n} = \epsilon_i$ in density-functional theory. *Phys. Rev. B.* **18** (1978), 187165–187168.

[57] R. O. Jones and O. Gunnarsson. The density functional formalism, its applications and prospects. *Rev. Mod. Phys.* **61** (1989), 689–746. DOI: 10.1103/RevModPhys.61.689.

[58] S. Kurth and J. P. Perdew. Role of the exchange-correlation energy: Nature's glue. *International Journal of Quantum Chemistry* **77** (2000), 814–818. DOI: 10.1002/(SICI)1097-461X(2000)77:5<814::AID-QUA3>3.0.CO;2-F.

[59] J. Perdew and K. Schmidt. "Jacob's ladder of density functional approximations for the exchange-correlation energy". *Density functional theory and its application to materials*. Ed. by VanDoren, V and VanAlsenoy, C and Geerlings, P. Vol. 577. AIP Conference Proceedings. 2001, 1–20.

[60] J. P. Perdew, K. Burke, and M. Ernzerhof. Generalized gradient approximation made simple. *Phys. Rev. Lett.* **77** (1996), 3865–3868.

[61] J. P. Perdew, K. Burke, and Y. Wang. Generalized gradient approximation for the exchange-correlation hole of a many-electron system. *Phys. Rev. B* **54** (1996), 16533–16539. DOI: 10.1103/PhysRevB.54.16533.

[62] J. Tao et al. Climbing the density functional ladder: Nonempirical meta–generalized gradient approximation designed for molecules and solids. *Phys. Rev. Lett.* **91** (2003), 1464011–1464014. DOI: 10.1103/PhysRevLett.91.146401.

[63] A. D. Becke. Density-functional thermochemistry. III. The role of exact exchange. *The Journal of Chemical Physics* **98** (1993), 5648–5652. DOI: 10.1063/1.464913.

[64] J. P. Perdew and W. Yue. Accurate and simple density functional for the electronic exchange energy: Generalized gradient approximation. *Phys. Rev. B* **33** (1986), 8800–8802. DOI: 10.1103/PhysRevB.33.8800.

[65] G. Pacchioni. First principles calculations on oxide-based heterogeneous catalysts and photocatalysts: Problems and advances. *Catalysis Letters* **145** (2015), 80–94. DOI: 10.1007/s10562-014-1386-2.

[66] K. Berland et al. van der Waals forces in density functional theory: a review of the vdW-DF method. *Reports on Progress in Physics* **78** (2015), 066501–066541. DOI: 10.1088/0034-4885/78/6/066501.

[67] A. Tkatchenko and M. Scheffler. Accurate Molecular Van Der Waals Interactions from Ground-State Electron Density and Free-Atom Reference Data. *Phys. Rev. Lett.* **102** (2009), 0730051–0730054. DOI: 10.1103/PhysRevLett.102.073005.

[68] S. Grimme. Semiempirical GGA-type density functional constructed with a long-range dispersion correction. *Journal of Computational Chemistry* **27** (2006), 1787–1799. DOI: 10.1002/jcc.20495.

[69] S. Grimme et al. A consistent and accurate ab initio parametrization of density functional dispersion correction (DFT-D) for the 94 elements H-Pu. *The Journal of Chemical Physics* **132** (2010), 15410401–15410419. DOI: 10.1063/1.3382344.

[70] F. Bloch. Über die Quantenmechanik der Elektronen in Kristallgittern. *Zeitschrift für Physik* **52** (1929), 555–600. DOI: 10.1007/BF01339455.

[71] N. Ashcroft and N. Mermin. *Solid State Physics*. Philadelphia: Saunders College, 1976.

[72] J. Singleton. *Band theory and electronic properties of solids*. Oxford master series in condensed matter physics. 2001.

[73] Monkhorst H. J., Pack J. D. Special points for Brillouin-zone integrations. *Phys. Rev. B* **13** (1976), 5188–5192.

[74] D. J. Chadi and M. L. Cohen. Special points in the brillouin zone. *Phys. Rev. B* **8** (1973), 5747–5753. DOI: 10.1103/PhysRevB.8.5747.

[75] R. M. Martin. *Electronic Structure: Basic Theory and Practical Methods*. Cambridge University Press, 2004. DOI: 10.1017/CBO9780511805769.

[76] Blochl P. E. Projector augmented-wave method. *Phys. Rev. B* **50** (1994), 17953–17979.

[77] G. Henkelman, B. Uberuaga, and H. Jonsson. A climbing image nudged elastic band method for finding saddle points and minimum energy paths. *J. Chem. Phys* **113** (2000), 9901–9904. DOI: 10.1063/1.1329672.

[78] F. Jensen. *Introduction to computational chemistry*. USA: John Wiley & Sons, Inc., 2006.

[79] K. Reuter and M. Scheffler. Composition, structure, and stability of RuO_2(110) as a function of oxygen pressure. *Phys. Rev. B* **65** (2002), 0354061–03540611. DOI: 10.1103/PhysRevB.65.035406.

[80] Q. Sun, K. Reuter, and M. Scheffler. Effect of a humid environment on the surface structure of RuO_2(110). *Phys. Rev. B* **67** (2003), 2054241–2054247. DOI: 10.1103/PhysRevB.67.205424.

[81] P. J. Linstrom and W. G. Mallard. *NIST Chemistry WebBook;NIST Standard Reference Database Number 69; National Institute of Standards and Technology:*

Gaithersburg, MD, http://webbook.nist.gov. [Online; Accessed 10-October-2017]. 2005.

[82] S. Hofmann. *Auger-and X-ray photoelectron spectroscopy in materials science*. Vol. 49. Springer Series in Surface Sciences. Berlin, Heidelberg: Springer-Verlag, 2013. DOI: 10.1007/978-3-642-27381-0.

[83] B. Johansson and N. Mårtensson. Core-level binding-energy shifts for the metallic elements. *Phys. Rev. B* **21** (1980), 4427–4457. DOI: 10.1103/PhysRevB.21.4427.

[84] L. Köhler and G. Kresse. Density functional study of CO on Rh(111). *Phys. Rev. B* **70** (2004), 1654051–1654059. DOI: 10.1103/PhysRevB.70.165405.

[85] V. Nilsson et al. Trends in adsorbate induced core level shifts. *Surf. Sci.* **640** (2015), 59–64. DOI: 10.1016/j.susc.2015.03.019.

[86] N. Mårtensson and A. Nilsson. On the origin of core-level binding energy shifts. *Journal of Electron Spectroscopy and Related Phenomena* **75** (1995), 209–223. DOI: 10.1016/0368-2048(95)02532-4.

[87] M. Van den Bossche et al. Effects of non-local exchange on core level shifts for gas-phase and adsorbed molecules. *The Journal of Chemical Physics* **141** (2014), 0347061–0347066. DOI: 10.1063/1.4889919.

[88] G. Henkelman, A. Arnaldsson, and H. Jonsson. A fast and robust algorithm for Bader decomposition of charge density. *Comput. Mater. Sci* **36** (2006), 354–360. DOI: 10.1016/j.commatsci.2005.04.010.

[89] R. F. W. Bader. The zero-flux surface and the topological and quantum definitions of an atom in a molecule. *Theoretical chemistry accounts* **105** (2001), 276–283. DOI: 10.1007/s002140000233.

[90] E. Sanville et al. Improved grid-based algorithm for Bader charge allocation. *Journal of computational chemistry* **28** (2007), 899–908. DOI: 10.1002/jcc.20575.

[91] W. Tang, E. Sanville, and G. Henkelman. A grid-based Bader analysis algorithm without lattice bias. *Journal of physics: Condensed matter* **21** (2009), 0842041–0842047. DOI: 10.1088/0953-8984/21/8/084204.

[92] A. P. Sutton. *Electronic structure of materials*. Oxford, UK: Oxford university press, 1993.

[93] L. C. Grabow and M. Mavrikakis. Mechanism of methanol synthesis on Cu through CO_2 and CO hydrogenation. *ACS Catalysis* **1** (2011), 365–384. DOI: 10.1021/cs200055d.

[94] P. B. Rasmussen, P. A. Taylor, and I. Chorkendroff. The interaction of carbon dioxide with Cu(100). *Surf. Sci.* **269/270** (1992), 352–359. DOI: 10.1016/0039-6028(92)91274-F.

[95] G. Chinchen et al. Mechanism of methanol synthesis from $CO_2/CO/H_2$ mixtures over copper/zinc oxide/alumina catalysts: use of14C-labelled reactants. *Applied Catalysis* **30** (1987), 333–338. DOI: 10.1016/S0166-9834(00)84123-8.

[96] J. Nakamura et al. Comment on "Active sites for CO_2 hydrogenation to methanol on Cu/ZnO catalysts". *Science* **357** (2017). DOI: 10.1126/science.aan8074.

[97] S. Kattel et al. Catalysis active sites for CO_2 hydrogenation to methanol on Cu/ZnO catalysts. *Science* **355** (2017), 1296–1299. DOI: 10.1126/science.aal3573.

[98] T. Bielz et al. Hydrogen on In_2O_3: reducibility, bonding, defect formation, and reactivity. *J. Phys. Chem. C* **114** (2010), 9022–9029. DOI: 10.1021/jp1017423.

[99] C. Gattinoni and A. Michaelides. Atomistic details of oxide surfaces and surface oxidation: the example of copper and its oxides. *Surf. Sci. Rep.* **70** (2015), 424–447. DOI: {10.1016/j.surfrep.2015.07.001}.

[100] M. Braithwaite, R. Joyner, and M. Roberts. Interaction of Oxygen with Cu(100) studied by low-energy electron-diffraction (LEED) and X-ray photoelectron-spectroscopy (XPS). *Farady Dicuss.* **60** (1975), 89–101. DOI: 10.1039/dc9756000089.

[101] M. Lampimaki et al. Nanoscale oxidation of Cu(100): Oxide morphology and surface reactivity. *J.Chem.Phys.* **126** (2007), 0347031–0347037. DOI: {10.1063/1.2424932}.

[102] K. Lahtonen et al. Oxygen adsorption-induced nanostructures and island formation on Cu{100}: Bridging the gap between the formation of surface confined oxygen chemisorption layer and oxide formation. *J.Chem.Phys.* **129** (2008), 1247031–1247039. DOI: 10.1063/1.2980347.

[103] M. Kittel et al. The structure of oxygen on Cu(100) at low and high coverages. *Surf. Sci.* **470** (2001), 311–324. DOI: 10.1016/S0039-6028(00)00873-6.

[104] T. Fujita et al. Phase boundaries of nanometer scale c(2x2)-O domains on the Cu(100) surface. *Phys. Rev. B* **54** (1996), 2167–2174. DOI: 10.1103/PhysRevB.54.2167.

[105] T. Fujita, Y. Okawa, and K. Tanaka. STM study of preferential growth of one-dimensional nickel islands on a Cu(100)-(2 root 2 X root 2)R45 degrees-0 surface. *Appl. Surf. Sci.* **130** (1998), 491–496. DOI: {10.1016/S0169-4332(98)00066-X}.

[106] P. B. Rasmussen et al. Methanol synthesis on Cu(100) from a binary gas mixture of CO_2 and H_2. *Catalysis Letters* **26** (1994), 373–381. DOI: 10.1007/BF00810611.

[107] J. Nakamura et al. "Model studies of methanol synthesis on copper catalysts". *11th International Congress On Catalysis - 40th Anniversary*. Ed. by J. W. Hightower et al. Vol. 101. Studies in surface science and catalysis. Elsevier, 1996, pp. 1389–1399. DOI: 10.1016/S0167-2991(96)80351-X.

[108] P. L. Hansen et al. Atom-resolved imaging of dynamic shape changes in supported copper nanocrystals. *Science* **295** (2002), 2053–2055. DOI: 10.1126/science.1069325.

[109] H. Tillborg et al. O/Cu(100) Studied by core level spectroscopy. *Surf. Sci.* **269** (1992), 300–304. DOI: 10.1016/0039-6028(92)91264-C.

[110] B. J. Lindberg et al. Molecular Spectroscopy by Means of ESCA II.Sulfur compounds. Correlation of electron binding energy with structure. *Physica Scripta* **1** (1970), 286–298. DOI: 10.1088/0031-8949/1/5-6/020.